THE ANTENNA LABORATORY

RESEARCH ACTIVITIES in ---

Automatic Controls   Antennas   Echo Are
Microwave Circuits   Astronautics E M Fiel
Terrain Investigations Radomes   Systems A
Wave Propagation   Submillim

N67 12984
(ACCESSION NUMBER)   (THRU)
88
(PAGES)   (CODE)
(NASA CR OR TMX OR AD NUMBER)   07
                                  (CATEGORY)

CR- 66234

THE REFLECTION COEFFICIENT OF A TEM MODE PARALLEL-PLATE WAVEGUIDE ILLUMINATING A PERFECTLY REFLECTING SHEET

Leonard L. Tsai

Grant No. NGR-36-008-048

2143-1   25 August 1966

Prepared for:
National Aeronautics and Space Administration
Washington, D.C. 20546

Department of ELECTRICAL ENGINEERING

THE OHIO STATE UNIVERSITY
RESEARCH FOUNDATION
Columbus , Ohio

NOTICES

When Government drawings, specifications, or other data are used for any purpose other than in connection with' a definitely related Government procurement operation, the United States Government thereby incurs no responsibility nor any obligation whatsoever, and the fact that the Government may have formulated, furnished, or in any way supplied the said drawings, specifications, or other data, is not to be regarded by implication or otherwise as in any manner licensing the holder or any other person or corporation, or conveying any rights or permission to manufacture, use, or sell any patented invention that may in any way be related thereto.

The Government has the right to reproduce, use, and distribute this report for governmental purposes in accordance with the contract under which the report was produced. To protect the proprietary interests of the contractor and to avoid jeopardy of its obligations to the Government, the report may not be released for non-governmental use such as might constitute general publication without the express prior consent of The Ohio State University Research Foundation.

Qualified requesters may obtain copies of this report from the Defense Documentation Center, Cameron Station, Alexandria, Virginia. Department of Defense contractors must be established for DDC services, or have their "need-to-know" certified by the cognizant military agency of their project or contract.

REPORT
by
THE OHIO STATE UNIVERSITY RESEARCH FOUNDATION
COLUMBUS, OHIO 43212

Investigation of | Theoretical and Experimental Studies of
Antennas for Reflectometer Application

Subject of Report | The Reflection Coefficient of a TEM Mode
Parallel-Plate Waveguide Illuminating a
Perfectly Reflecting Sheet

Submitted by | Leonard L. Tsai
Antenna Laboratory
Department of Electrical Engineering

Date | 25 August 1966

The material contained in this report is also used as a
Thesis submitted to the Department of Electrical
Engineering, The Ohio State University as partial
fulfillment for the degree Master of Science.

ACKNOWLEDGEMENTS

ABSTRACT

The reflection coefficient of a parallel-plate waveguide operating in the TEM mode and illuminating a perfectly conducting sheet is analyzed as a function of guide aperture to reflector distance by using wedge diffraction techniques. For the half-plane guide, the reflection coefficient is easily obtained by integrating the reflected field over the guide aperture. For guides with finite wedge angles less than 90°, the reflection coefficient is found by assuming that the interactions between the guide aperture and reflecting sheet are bouncing plane waves and obtaining them through the Higher-Order Diffraction Concept. For ground plane mounted guides, the reflection coefficient is obtained through an iterative process of successively bouncing cylindrical waves.

CONTENTS

CONTENTS (Cont.)

CHAPTER I
INTRODUCTION

A. Statement of the Problem

Wedge diffraction theory is used in this analysis to calculate

the aperture admittance of a TEM parallel-plate waveguide illuminat-

ing an infinite perfectly reflecting sheet. The general geometry of

the problem is as shown in Fig. 1. The parallel-plate waveguide is
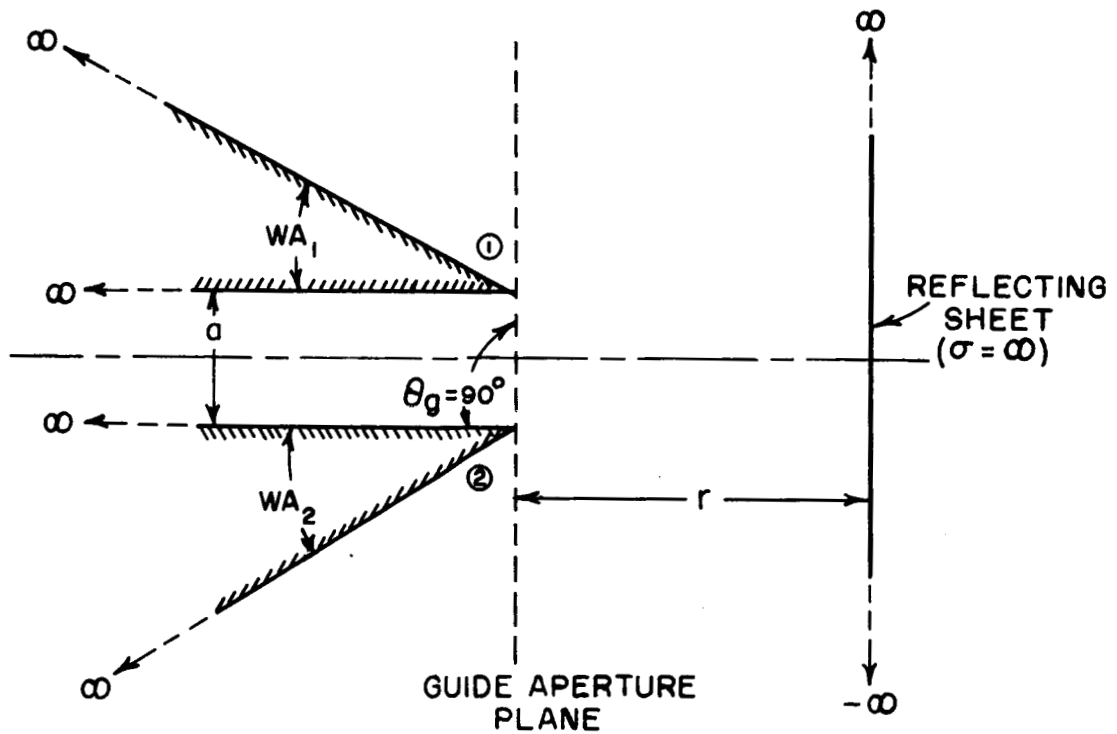
Fig. 1. Parallel-plate waveguide illuminating
a reflecting sheet.

1

constructed from two perfectly conducting wedges of arbitrary wedge angles WA_1 and WA_2 and separated by the guide width (a). For simplicity of analysis, the guide truncation angle θ_g is chosen to be 90° and the reflecting sheet is oriented perpendicular to the guide axis. The reflection coefficient inside the parallel-plate waveguide is then calculated as a function of the distance to the reflecting sheet (r).

This analysis is the first step of an attempt to gain further insight into the plasma measurement problem during space craft re-entry. Although infinite parallel-plate waveguides are hardly practical as space craft mounted antennas, this simplified analysis does serve to demonstrate the basic diffraction mechanisms involved between the critical layer of a reflecting plasma and the vehicle skin in which a reflectometer system would be mounted. This basic two-dimensional problem gives insight into the more practical three-dimensional problem.

B. <u>Wedge Diffraction Theory</u>

The principal method employed in this analysis is diffraction by a conducting wedge. The diffraction of a plane wave by a wedge was first solved by Sommerfeld.[1] Pauli obtained a practical formulation of the solution for a finite-angle conducting wedge.[2]

The total diffracted electromagnetic field from the wedge may be treated as the superposition of the geometrical optics field and the

2

diffracted field which behaves as a cylindrical wave radiating from the edge of the wedge. Therefore, the techniques of ray optics can be used with which the field can be determined from the diffracted rays from the edge and the geometrical optics rays. A diffraction function, V_B, introduced by Pauli is employed in the analysis and is given in Appendix A.

The diffraction of a plane wave by a wedge is shown in Fig. 2. The solution to the plane wave diffraction problem may be expressed in terms of a scalar function that represents the component of the electromagnetic field normal to the plane of study in Fig. 2. The
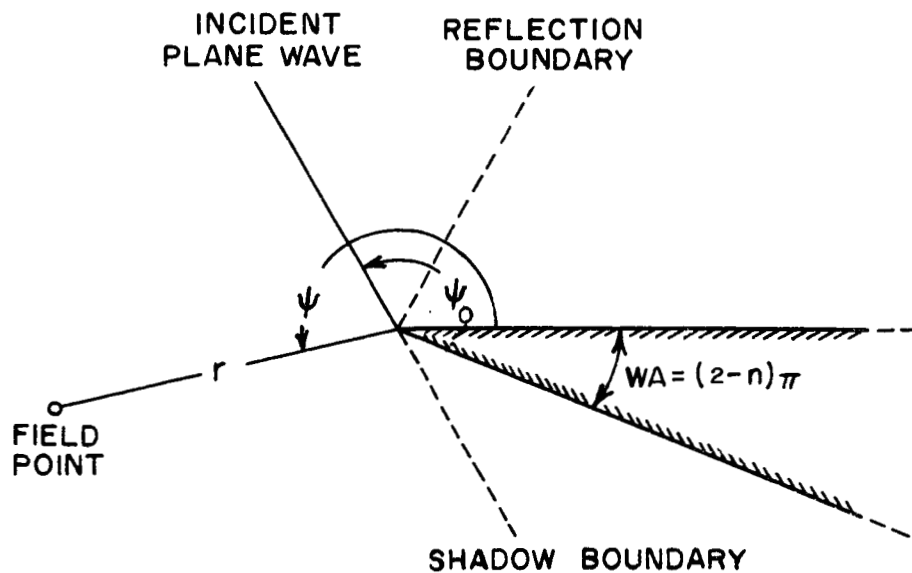
Fig. 2. Geometry for wedge diffraction.

total field may be expressed as

(1) $U = U_o + U_d$,

where U_o is the geometrical optics field and U_d is the diffracted field. The diffracted field is given by

(2) $U_d = V_B(r, \psi - \psi_o, n) + V_B(r, \psi + \psi_o, n)$,

where the electric field polarization is perpendicular to the edge of the wedge. The geometrical optics field is defined in three regions, as shown in Fig. 3. For plane wave incidence, the geometrical optics fields are

INCIDENT WAVE

INCIDENT REGION

INCIDENT AND REFLECTED REGION

$WA = (2 - n)\pi$

INCIDENT REGION
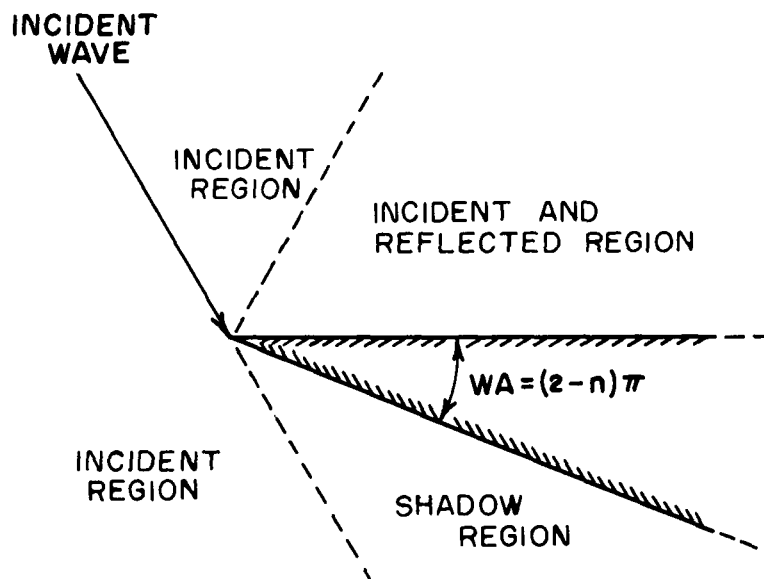
SHADOW REGION

Fig. 3. Geometrical optics regions.

4

(3a) $U_O = e^{jkr \cos(\psi - \psi_O)}$,   incident region;

(3b) $U_O = e^{jkr \cos(\psi - \psi_O)} + e^{jkr \cos(\psi + \psi_O)}$,

incident and reflected region; and

(3c) $U_O = 0$, shadow region.

The time dependence, $e^{j\omega t}$, is used throughout this analysis.

The diffracted wave U_d may be represented as a cylindrical wave radiating from the edge (see Eq. (80) in Appendix A). In fact, at large distances from the edge in regions removed from shadow boundaries U_d has the radial dependence $e^{-jkr}/\sqrt{r}$. Because of this cylindrical nature, subsequent diffraction of a diffracted wave may be treated as the diffraction of a cylindrical wave by a wedge.

The diffraction of a cylindrical wave by a wedge is illustrated in Fig. 4. The geometrical optics field in this case is given by

(4a) $U_O = \dfrac{e^{-jkR}}{\sqrt{R}} = \dfrac{e^{-jk[r^2 + r_O^2 - 2rr_O \cos(\psi - \psi_O)]^{\frac{1}{2}}}}{[r^2 + r_O^2 - 2rr_O \cos(\psi - \psi_O)]^{\frac{1}{4}}}$,

incident region;

(4b) $U_O = \dfrac{e^{-jkR}}{\sqrt{R}} + \dfrac{e^{-jkR'}}{\sqrt{R'}}$

$= \dfrac{e^{-jk[r^2 + r_O^2 - 2rr_O \cos(\psi - \psi_O)]^{\frac{1}{2}}}}{[r^2 + r_O^2 - 2rr_O \cos(\psi - \psi_O)]^{\frac{1}{4}}}$

$+ \dfrac{e^{-jk[r^2 + r_O^2 - 2rr_O \cos(\psi + \psi_O)]^{\frac{1}{2}}}}{[r^2 + r_O^2 - 2rr_O \cos(\psi + \psi_O)]^{\frac{1}{4}}}$,

incident and reflected region; and
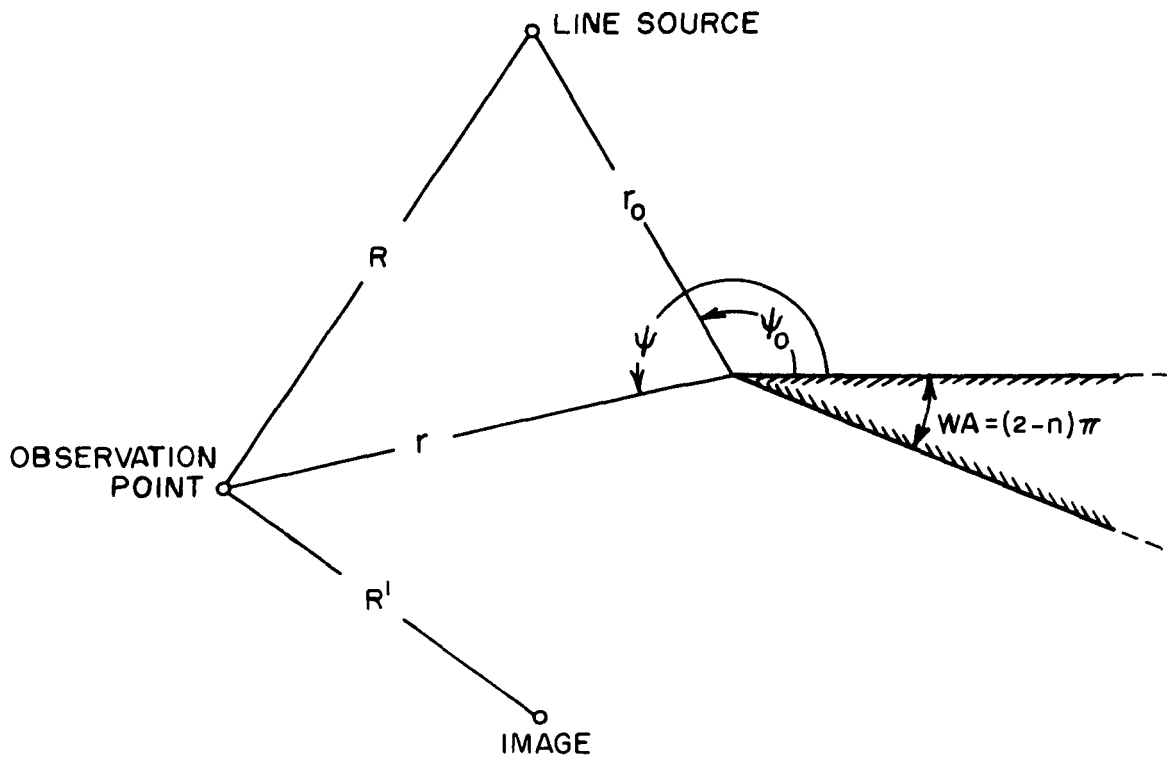
Fig. 4. Line source near-field diffraction.

(4c) $U_O = 0$, shadow region,

where R and R' are the respective distances of the line source and its image to the observation point. The regions for the geometrical optics fields are the same as those shown in Fig. 3. The diffracted field is obtained by modifying the solution given by Obha[3] for the diffraction of a half-plane illuminated by a dipole source. This solution has been reduced to the two-dimensional form and extended

to wedge diffraction. The diffracted wave is thus given by

$$
(5) \qquad U_d(r, r_o, \psi, \psi_o, n) = \frac{e^{-jk(r+r_o)}}{\sqrt{r+r_o}} \; e^{jk\frac{rr_o}{r+r_o}} \; \times
$$

$$
\left[V_B\left(\frac{rr_o}{r+r_o}, \psi-\psi_o, n\right) + V_B\left(\frac{rr_o}{r+r_o}, \psi+\psi_o, n\right) \right] \; .
$$

Equation (1) then gives the total field.

The far-zone diffracted field of an incident cylindrical wave $(r >> r_o)$ is given through Eq. (5) as

$$
(6) \qquad U_d = \frac{e^{-jkr}}{\sqrt{r}} \left[V_B(r_o, \psi-\psi_o, n) + V_B(r_o, \psi+\psi_o, n) \right] \; .
$$

Equation (6) may also be obtained by applying reciprocity to Eq. (2).[4]

Equation (5), an approximate solution to the line source diffraction problem, was compared with an exact eigenfunction formulation and demonstrated to be quite accurate in its regions of applicability.[5] The diffraction functions, Eqs. (2) and (5), have been demonstrated to be quite useful through their applications in a number of antenna problems.[6,7,8,9]

C. TEM Waveguide Mode

The TEM mode in the parallel-plate waveguide may be represented as a plane wave propagating in the guide as shown in Fig. 5. For this mode the field distribution across the guide is uniform, with the electric field polarization perpendicular to the guide walls. For
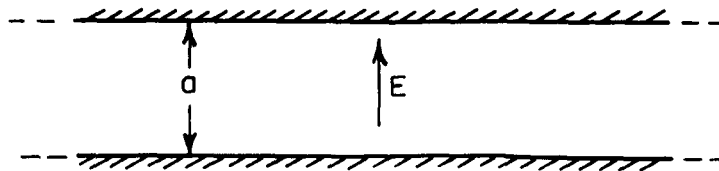
Fig. 5. TEM mode propagation.

a unit amplitude magnetic field parallel to the guide walls, integration

of the Poynting vector, which is uniform across the guide, over the

guide cross section yields a power flow per unit depth of the guide as

$(Z_o a)$, where (Z_o) is the impedance of free space and (a) is the width

of the guide.

In conventional transmission line theory, power flow may be

represented in terms of circuit theory concepts as the product of

modal current and modal voltage. These modal quantities are

related by the transmission line impedance. For the TEM mode the

transmission line impedance is simply the ratio of the electric to the

magnetic fields, or in this case the impedance of free space (Z_o).

The magnetic field for the TEM mode may be represented by a scalar

function. Therefore, for a guide operating in the TEM mode with a

guide width (a), in which the magnetic field has unit amplitude and

zero phase reference, the modal circuit quantities are given by

(7) $\qquad I_O = \sqrt{a}$

and

$$V_O = \sqrt{a}\ Z_O\ .$$

D. Reflection Coefficient by Wedge Diffraction

By wedge diffraction theory the near field of a TEM parallel-plate waveguide may be readily determined. For the half-plane guide, the reflection coefficient may be obtained by integrating over the guide aperture the field reflected by the reflecting sheet. For guides with finite wedge angles less than $90°$, interactions between the guide aperture and the reflecting sheet may be approximated by bouncing plane waves. Wedge diffraction theory is used then to compute the coupling between these plane waves and the guide, hence the reflection coefficient of the guide. For ground plane mounted guides, the exact nature of the interactions between the guide and the reflecting sheet may be taken into account in a method of successively bouncing cylindrical waves. Wedge diffraction theory then gives the coupling between these cylindrical waves and the guide.

For each of the above cases, normalized admittances may be readily obtained from the corresponding reflection coefficients.

CHAPTER II
PARALLEL-PLATE WAVEGUIDE CHARACTERISTICS

Some of the characteristics of the parallel-plate waveguide

pertinent to the reflection coefficient analysis is treated in this

chapter.

A. Near-Zone Field

The near-zone fields of the guide in Fig. 6 are discussed in

this section. The diffraction from the guide aperture is treated by

superimposing the diffracted fields from each of the wedges. The

singly diffracted fields are caused by the unit amplitude incident

plane wave inside the guide. In regions sufficiently removed from

the shadow boundaries of the incident wave, the singly diffracted

fields may be represented by rays that have only angular dependence

because the radial and angular dependences of these singly diffracted

fields are separable. The singly diffracted wave from edge 1,

represented by the ray $R_1^{(1)}$, is given through

$$(8) \qquad R_1^{(1)}(\theta) = \frac{1}{n_1} \sin \frac{\pi}{n_1} \left(\frac{1}{\cos \frac{\pi}{n_1} - \cos \frac{\pi + \theta}{n_1}} \right) \qquad ,$$

where the factor

Fig. 6. TEM mode parallel-plate waveguide.

$$\frac{e^{-j\left(kr + \frac{\pi}{4}\right)}}{\sqrt{2\pi kr}}$$

is suppressed because only angular variations are of interest.

Superscripts denote the order of diffraction in this chapter. Similarly the singly diffracted wave from edge 2, represented by the ray $R_2^{(1)}$, is given through

(9)
$$R_2^{(1)}(\theta) = \frac{1}{n_2} \sin \frac{\pi}{n_2} \left(\frac{1}{\cos \dfrac{\pi}{n_2} - \cos \dfrac{\pi - \theta}{n_2}} \right) \quad .$$

11

The relation between the ray and the magnetic field is given later in Eq. (17).

The singly diffracted ray from edge 1 in the direction of edge 2 is given by

$$(10) \qquad R_1G^{(1)}(\theta = -\theta_g) = \frac{1}{n_1} \sin \frac{\pi}{n_1} \left(\frac{1}{\cos \frac{\pi}{n_1} - \cos \frac{\pi - \theta_g}{n_1}} \right) \qquad .$$
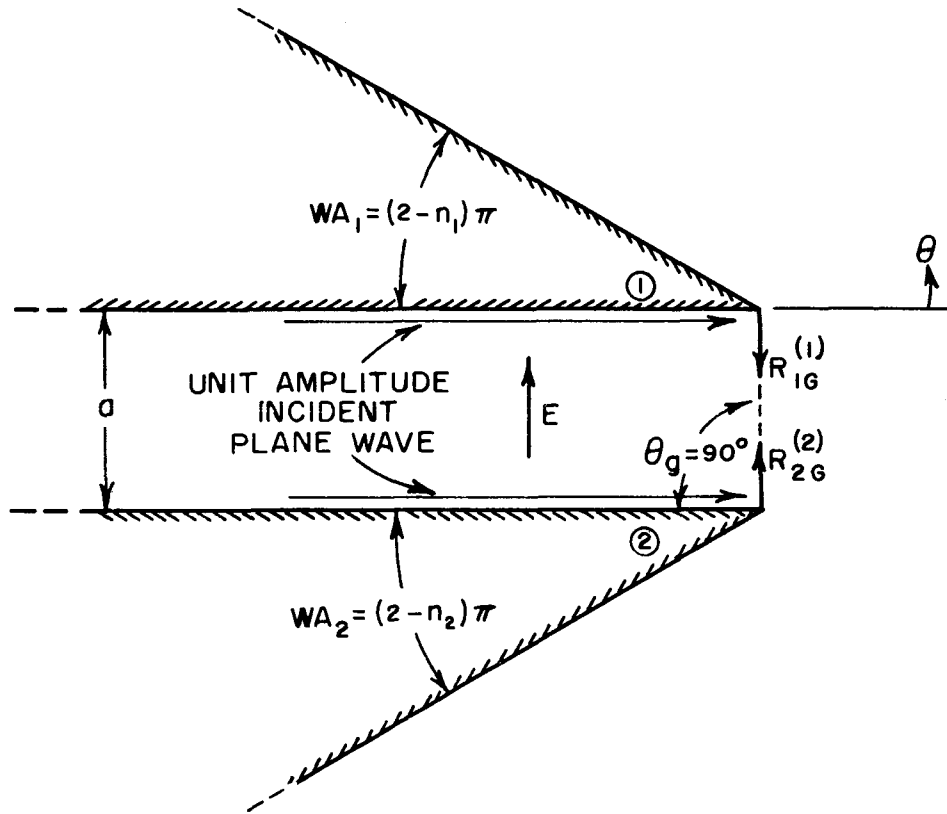
Similarly the singly diffracted ray from edge 2 in the direction of edge 1 is given by

$$(11) \qquad R_2G^{(1)}(\theta = \pi - \theta_g) = \frac{1}{n_2} \sin \frac{\pi}{n_2} \left(\frac{1}{\cos \frac{\pi}{n_2} - \cos \frac{\theta_g}{n_2}} \right) \qquad .$$

These singly diffracted rays will be used in finding the doubly diffracted fields from the edges.

The singly diffracted wave from each edge may be again diffracted by the other wedge producing doubly diffracted rays. The doubly diffracted rays may be diffracted again by the edges and so on producing higher-order interactions between the wedges.

Inclusion of contributions by higher-order diffractions may be achieved by applying the "Higher-Order Diffraction Concept".[6,7] However, for $\theta_g = 90°$, the singly diffracted wave $R_1^{(1)}$ radiating in the direction of edge 2 has a reflection shadow boundary back in the direction of interest as shown in Fig. 7. The doubly diffracted wave $R_2^{(2)}$ from edge 2 in the direction of edge 1 is not representable as a

12
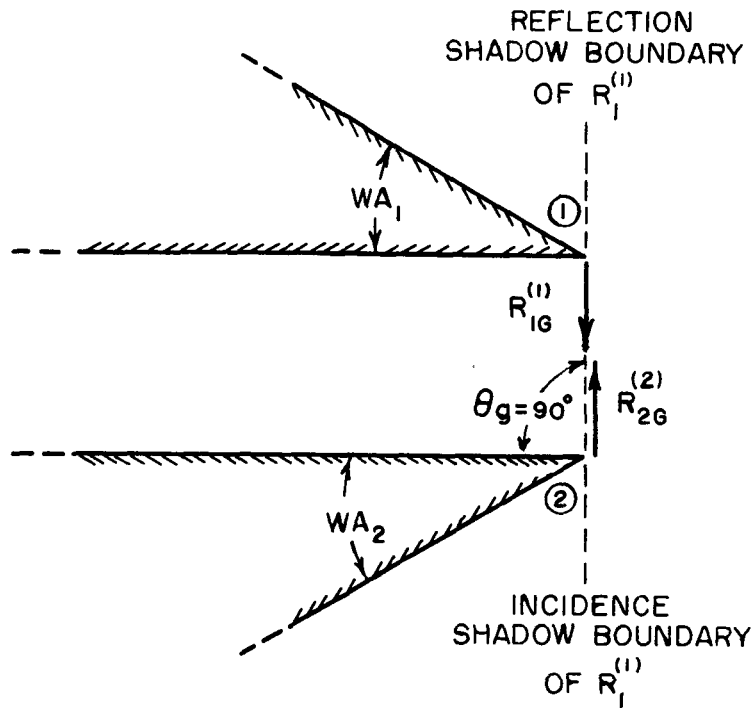
Fig. 7. Shadow boundary of aperture diffracted wave.

cylindrical wave near the shadow boundary of $R_1^{(1)}$. Thus the third

order diffracted wave $R_1^{(3)}$ from edge 1 cannot be accurately described

by the uniform cylindrical wave diffraction relationship of Eq. (6). The

same relationship holds between $R_1^{(2)}$ and $R_2^{(3)}$. Similar shadow

boundaries for subsequent diffractions then render higher order wedge

interactions inaccurate for $\theta_g = 90°$ by the uniform wave diffraction

functions. For guide widths larger than $\lambda/4$, however, inclusion of

no higher than the doubly diffracted contributions gives quite accurate

results everywhere except near the guide aperture plane.[6, 10]

13

The near-zone magnetic field plot is obtained for the geometry

of Fig. 8 in the following manner: The origin of the x-y coordinates is

assigned to edge 1, with r_1 and r_2 denoting the distances from the
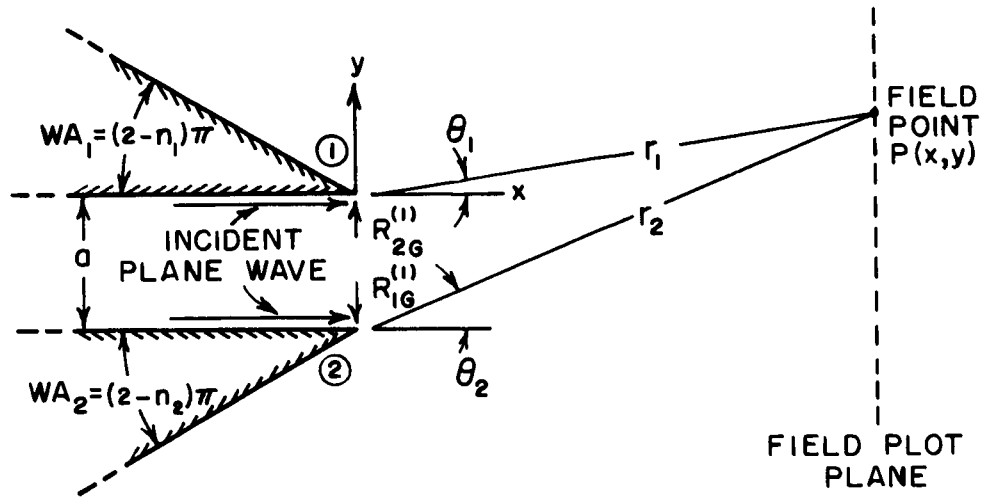
Fig. 8. Near-zone field plot geometry.

field point P(x, y) to edges 1 and 2, respectively. The angles θ_1 and

θ_2 are defined with respect to the guide axis, with

$$\theta_1 = \tan^{-1} \frac{y}{x} \quad \text{and} \quad \theta_2 = \tan^{-1} \frac{y+a}{x} \quad .$$

Assuming a unit amplitude magnetic field incident inside

the waveguide, the singly diffracted magnetic field from edge 1

at the field point P(x, y) is given by

$$(12) \qquad H_1^{(1)}(P) = V_B(r_1, \pi + \theta_1, n_1) \quad .$$

14

The singly diffracted field from edge 2 is given by

$$(13) \qquad H_2^{(1)}(P) = V_B(r_2, \pi - \theta_2, n_2) \ .$$

The doubly diffracted field from edge 1 results from the singly diffracted ray $R_2G^{(1)}$ from edge 2 and is given by the line source field diffraction relationship of Eq. (5) as

$$(14) \qquad H_1^{(2)}(P) = R_2G^{(1)} \cdot \frac{e^{-j\frac{\pi}{4}}}{\sqrt{2\pi k}} \times \frac{e^{jk\left[\frac{r_1 \cdot a}{r_1 + a} - (r_1 + a)\right]}}{\sqrt{r_1 + a}}$$

$$\times \left[V_B\left(\frac{r_1 \cdot a}{r_1 + a}, \theta_1 + \frac{\pi}{2}, n_1\right) + V_B\left(\frac{r_1 \cdot a}{a + r_1}, \frac{3\pi}{2} + \theta_1, n_1\right) \right] \ .$$

The doubly diffracted field from edge 2 results from $R_1G^{(1)}$ and is given by

$$(15) \qquad H_2^{(2)}(P) = R_1G^{(1)} \frac{e^{-j\frac{\pi}{4}}}{\sqrt{2\pi k}} \times \frac{e^{jk\left[\frac{r_2 \cdot a}{r_2 + a} - (r_2 + a)\right]}}{\sqrt{r_2 + a}}$$

$$\times \left[V_B\left(\frac{r_2 \cdot a}{r_2 + a}, \frac{\pi}{2} - \theta_2, n_2\right) \right.$$

$$\left. + V_B\left(\frac{r_2 \cdot a}{r_2 + a}, \frac{3\pi}{2} - \theta_2, n_2\right) \right] \ .$$

Since the incident wave from within the guide is plane, the geometrical optics field is given by

$$(16) \qquad H_G = e^{-jkx} \qquad -a \leq y \leq 0$$

$$\qquad\qquad\qquad 0 \qquad\qquad \text{otherwise} \ .$$

The total field $H_T(P)$ at $P(x,y)$ is then obtained through super-position as

$$(17) \qquad H_T(P) = H_1^{(1)}(P) + H_1^{(2)}(P) + H_2^{(1)}(P) + H_2^{(2)}(P) + H_G \quad .$$

B. Response of a Guide to a Line Source

Equivalent line sources with omni-directional patterns are employed in the subsequent analyses. The modal current I of an equivalent line source is related to its radiated magnetic field H and ray R by

$$(18) \qquad I\, \frac{e^{-jkr + j\frac{\pi}{4}}}{\sqrt{2\pi r}} = H = \frac{e^{-j\left(kr + \frac{\pi}{4}\right)}}{\sqrt{2\pi kr}}\, R \quad .$$

The response of a guide to an equivalent line source is obtained by reciprocity. As depicted in Fig. 9 the response of a guide to a

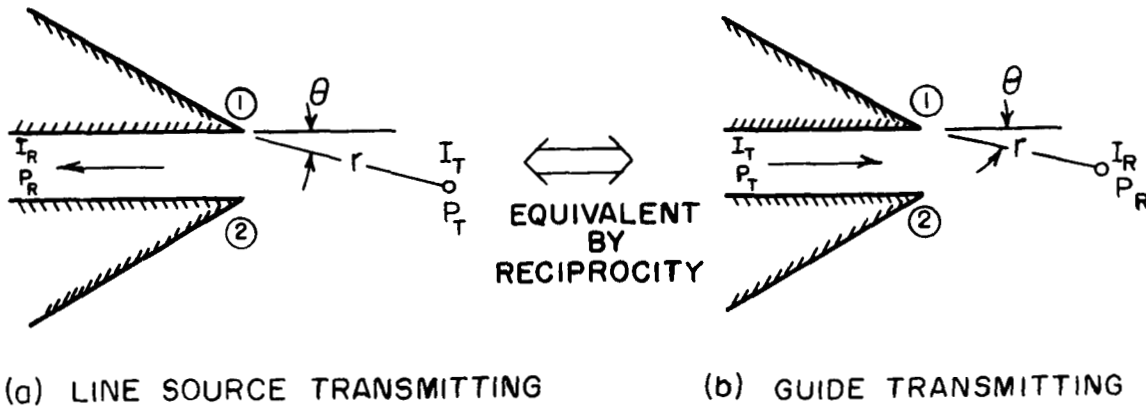(a) LINE SOURCE TRANSMITTING   (b) GUIDE TRANSMITTING

Fig. 9. Application of reciprocity to find the response of a guide to a line source.

16

line source is equal to the response of that line source to the guide

by reciprocity. In Fig. 9a a line source located a distance r away

from the guide transmits a power per unit length P_T, with associated

modal current I_T. The guide receives a power per unit length P_R

with associated modal current I_R from the line source. In the

reciprocal situation in Fig. 9b, the guide transmits the power P_T

with associated modal current I_T. The line source receives the

power P_R with an associated modal current I_R. The power received

by the line source in Fig. 9b is given by

$$(19) \qquad P_R = \frac{\lambda}{2\pi} \left| H_T(r,\theta) \right|^2 Z_o \quad,$$

where $\lambda/2\pi$ is the effective aperture of the line source and $H_T(r,\theta)$

is the field from the guide at the line source. Hence the modal

current received by the line source is given by

$$(20) \qquad I_R = \sqrt{\frac{\lambda}{2\pi}} \ H_T(r,\theta) \quad,$$

where the characteristic impedance of the line source is Z_o. The

modal current of the transmitting guide is $\sqrt{a}$ if the magnetic field

in the guide is of unit amplitude and the guide width is (a). The

response of the line source to the guide in Fig. 9b is then expressible

in terms of the modal current ratio

$$(21) \qquad \frac{I_R}{I_T} = \sqrt{\frac{\lambda}{2\pi a}} \ H_T(r,\theta) \quad.$$

By reciprocity, Eq. (21) gives the response I_R of a guide to a line source with a transmitting modal current I_T as depicted in Fig. 9a.

C. Self Reflection Coefficient

The reflection coefficient of the waveguide aperture with the waveguide radiating into free space is denoted as the "self reflection coefficient" of the waveguide. Extensive derivation of the self reflection coefficient is given for both TEM and TE_{01} parallel-plate waveguide apertures in Reference 10. The formulation of the TEM waveguide aperture admittance is based upon the symmetry of half-plane diffraction as shown in Fig. 10. Because of the symmetry of half-plane diffraction, the diffracted field distributions of Fig. 10a and b are identical except for sign. Therefore the power reflected back into the guide by aperture mismatch (Fig. 10a) is the same as

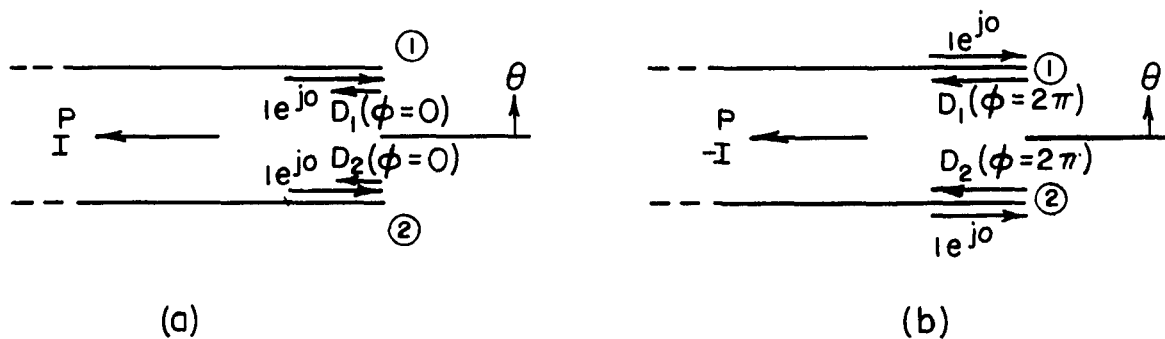(a)   (b)

Fig. 10. Plane wave incidence from inside
and outside the guide.

that received by the guide for a plane wave incident outside the guide from the $\theta = 180°$ direction (Fig. 10b). In order to determine the response of the guide to plane wave incidence, the effective aperture of the guide must be considered.

For the TEM mode guide the magnetic field intensity in the far-field region is accurately given by

(22) $$H_T(r, \theta) = \frac{e^{-j\left(kr + \frac{\pi}{4}\right)}}{\sqrt{2\pi kr}} \quad R_T(\theta) = \frac{e^{-jkr}}{\sqrt{r}} \quad D_T(\theta) \quad ,$$

where $H_T(\theta)$ is the field, $R_T(\theta)$ the ray, and $D_T(\theta)$ the diffraction coefficient associated with the guide. The antenna gain of the parallel-plate waveguide may be calculated from the conventional formula for two-dimensional gain,

(23) $$G = \frac{2\pi rS}{P_o} \quad ,$$

where S is the radiated power density at radius r and P_o is the total power per unit length incident in the transmitting guide. The power density is related to the radiated field of the guide by

(24) $$S = Z_o \left|H_T\right|^2 = \frac{Z_o}{r} \left|D_T\right|^2 = \frac{Z_o}{2\pi kr} \left|R_T\right|^2 \quad ,$$

where Z_o is the free-space impedance. Since the power incident in the TEM guide with a unit amplitude incident magnetic field is (aZ_o) where (a) is the guide width, the gain of the guide is given by

$$(25) \qquad G = \frac{1}{ka} \left| R_T \right|^2 = \frac{2\pi}{a} \left| D_T \right|^2 \; ,$$

where R_T and D_T are evaluated for the direction in which gain is to be determined. The effective aperture of the TEM parallel-plate waveguide is then given by

$$(26) \qquad W_e = \frac{\lambda}{2\pi} \; G = \frac{1}{k^2 a} \left| R_T \right|^2 = \frac{\lambda}{a} \left| D_T \right|^2 \; .$$

From Eqs. (22) and (25), the response of the guide to a plane wave of magnetic field intensity H_i is

$$(27) \qquad I = \sqrt{\frac{\lambda}{a}} \; D_T \; H_i \; e^{-j\frac{\pi}{4}} \; ,$$

where D_T is directly related to H_T from Eq. (17) in the far-field by Eq. (22). Equation (27) may also be obtained from Eq. (21). Thus the induced modal current in the guide corresponding to the reflected power caused by aperture mismatch in Fig. 10a is obtained from Eq. (27) as

$$(28) \qquad I = -\frac{1}{2} \sqrt{\frac{\lambda}{a}} \; [\, D_1 (\varphi = 2\pi) + D_2 (\varphi = 2\pi)] \; e^{-j\frac{\pi}{4}} \; ,$$

where the factor $1/2$ results from plane wave grazing incidence (where $H_i = 1/2$).[8] The minus sign results from the difference between Figs. 10a and b. Superposition is used to find the responses of the guide, D_1 and D_2, to the incident plane wave from outside the guide in Fig. 10b. The angle φ is used in the same convention as in

the diffraction function $V_B(r, \phi, n)$. The induced modal current may also be expressed as

$$(29) \qquad I = \frac{1}{2} \sqrt{\frac{\lambda}{a}} \; [\, D_1(\phi = 0) + D_2(\phi = 0)] \; e^{-j\frac{\pi}{4}} \qquad .$$

The self reflection coefficient, or reflection due to aperture mismatch for the TEM, parallel-plate, half-plane waveguide is given by

$$(30) \qquad \Gamma_0 = \frac{I}{I_0} = \frac{1}{2} \; \frac{\sqrt{\lambda}}{a} \; [\, D_1(\phi = 0) + D_2(\phi = 0)] \; e^{-j\frac{\pi}{4}} \qquad .$$

It should be noted that Eq. (30) may be obtained by simply considering the rays propagating back into the guide as shown in Fig. 11.
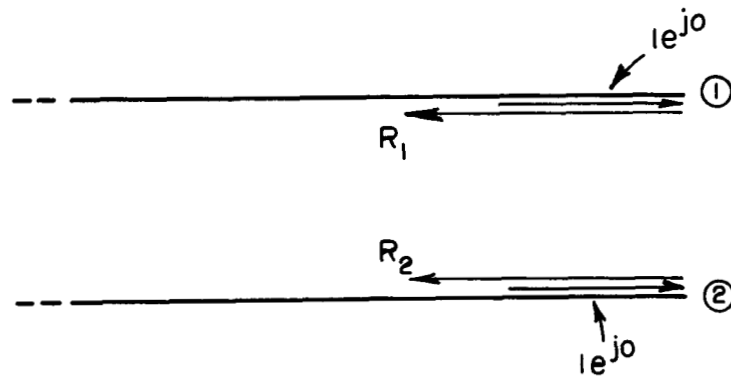
Fig. 11. Self-reflection coefficient ray diagram.

Normalized aperture admittance may then be obtained from the conventional relationship

$$(31) \qquad \frac{Y_A}{Y_o} = \frac{1 - \Gamma_o}{1 + \Gamma_o} \qquad .$$

Equation (30) is believed to be valid for guides composed of wedges with arbitrary wedge angles. Comparison between measured and calculated data has shown Eq. (30) to be correct in predicting the reflection coefficient due to aperture mismatch for guides of all wedge angles.[10]

CHAPTER III
APERTURE INTEGRATION APPROACH FOR
HALF-PLANE GUIDES

A. <u>Reflection Coefficient Analysis</u>

The reflection coefficient of a normally truncated half-plane

guide illuminating a reflecting sheet is discussed in this section.

Figure 12 shows the half-plane guide with a reflecting sheet located

Fig. 12. Half-plane guide illuminating a
reflecting sheet.

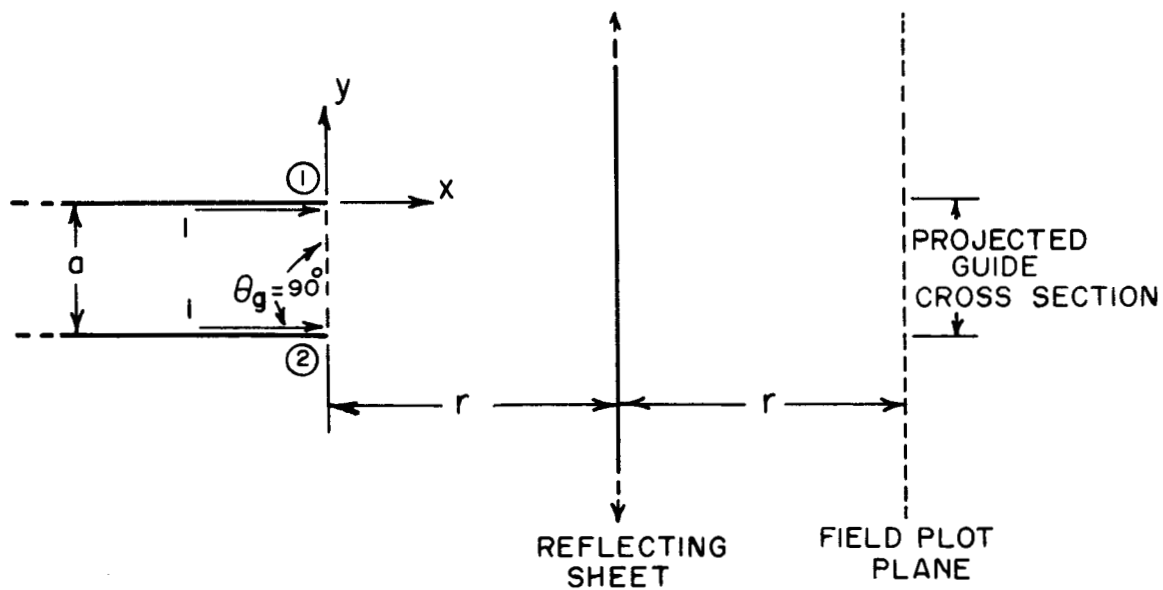a distance (r) away from the aperture. The near-zone field plot according to Section IIA was calculated for various guide widths, with the distance (2r) ranging from 0.1λ to 10.0λ. Table I gives the total magnetic field plot for a half-plane guide of 0.278λ guide width at field plot planes of 0.4λ, 2.0λ, and 5.0λ away from the guide aperture.

The magnetic field values in Table I indicate that the near field of the half-plane guide in the aperture cross section can be adequately represented as a plane wave because of its essentially uniform amplitude distribution and shallow phase curvature.

For the geometry of Fig. 12 the field plot of the free-space guide at $x = 2r$ is used to represent the reflected field from a reflecting sheet at $x = r$ incident on the guide aperture in the -x direction as shown in Fig. 13. In cases where the reflected wave H_r of Fig. 13a is plane, no further diffraction will occur because of its incidence on the aperture. Integration of the reflected field H_r at the guide aperture plane over the guide cross section yields the power received by the guide due to reflection at the reflecting sheet. Since $H_r = H_i$ in Fig. 13, the average field in the projected guide cross section in the field plot plane at (2r) in Fig. 13b, denoted by H_i (average), approximates the plane wave propagating back into the guide due to the reflection in Fig. 13a, H_r (average).

24

TABLE I

MAGNETIC FIELD OF A HALF-PLANE GUIDE WITH a = 0.278λ

y(λ)	2r = 0.4λ		2r = 2.0λ	
	Magnitude	Phase (in deg.)	Magnitude	Phase
-0.3058	0.40963	-114.3°	0.19678	41.6°
-0.2780	0.41918	-110.9°	0.19701	42.3°
-0.2502	0.42751	-108.1°	0.19721	42.9°
-0.2224	0.43434	-105.9°	0.19736	43.4°
-0.1946	0.43941	-104.4°	0.19747	43.8°
-0.1668	0.44254	-103.4°	0.19754	44.0°
-0.1390	0.44360	-103.1°	0.19756	44.0°
-0.1112	0.44254	-103.4°	0.19754	44.0°
-0.0834	0.43941	-104.4°	0.19747	43.8°
-0.0556	0.43434	-105.9°	0.19736	43.4°
-0.0278	0.42751	-108.1°	0.19721	42.9°
0.0000	0.41918	-110.9°	0.19701	42.3°
0.0278	0.40963	-114.3°	0.19678	41.6°

y(λ)	2r = 5.0λ	
	Magnitude	Phase
-0.3127	0.12451	43.5°
-0.2780	0.12454	43.9°
-0.2432	0.12457	44.2°
-0.2085	0.12458	44.5°
-0.1737	0.12459	44.6°
-0.1390	0.12460	44.6°
-0.1042	0.12459	44.6°
-0.0695	0.12458	44.5°
-0.0347	0.12457	44.2°
0.0000	0.12454	43.9°
0.0348	0.12451	43.5°
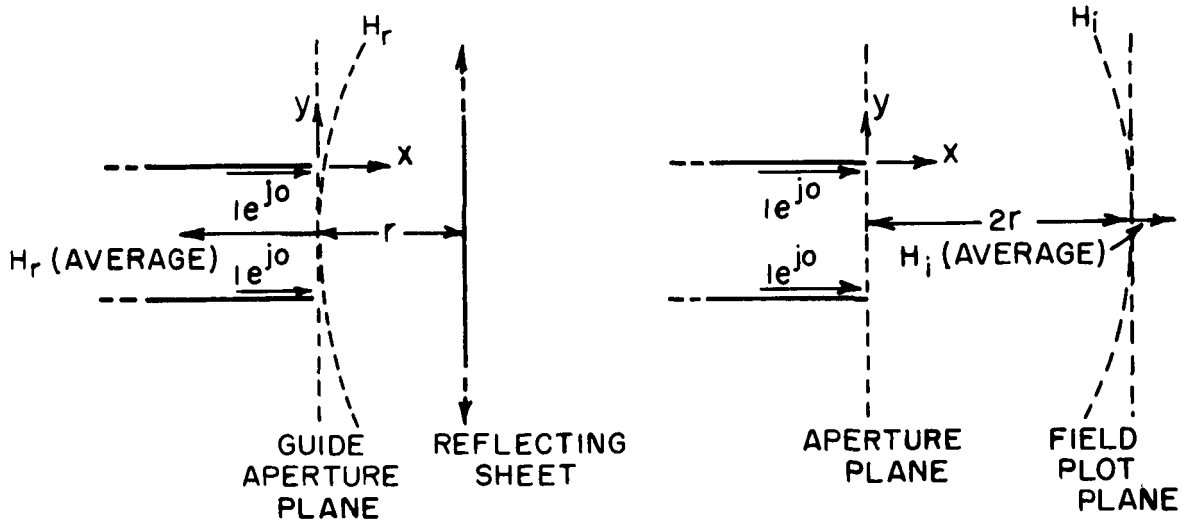
(a) REFLECTED WAVE H_r $H_r = H_i$ (b) FREE-SPACE WAVE H_i

Fig. 13. Reflected wave and equivalent free space wave
          for a half-plane guide.

If the plane wave incident on the guide edges from within the

guide has a unit amplitude magnetic field, the value of H_r (average)

is the reflection coefficient Γ_r of the guide due to the reflection by

the reflecting sheet. The total reflection coefficient is then the

phasor sum of the self reflection coefficient Γ_o from Eq. (30) and

Γ_r, thus

(32) $\Gamma_T = \Gamma_o + \Gamma_r$.

Γ_T represents the total reflection coefficient of a normally truncated, half-plane, parallel-plate waveguide illuminating a reflecting sheet with the phase reference of Γ_T at the guide aperture plane.

Calculation of Γ_r consists of first calculating the fields H_i at $x = 2r$ according to the method in Section IIA. Then the fields across the guide cross section are averaged to obtain H_i (average), and hence H_r (average).

B. Results

The computation of Γ_T is accomplished with the aid of a Scatran program on the IBM 7094 digital computer. Γ_T is calculated as a function of (r), the distance from the guide aperture to the reflecting sheet.

The reflection coefficient magnitude may be measured with a sectoral horn as shown in Fig. 14. The illustrated horn was constructed by flaring out one dimension of an X-band rectangular waveguide and keeping the other dimension fixed. Horns of this type have been found to simulate infinite parallel-plate waveguides quite adequately for the purposes of measuring radiation patterns,[11] coupling between parallel-plate waveguides,[8] and self reflection coefficients.[10] The reflecting sheet to waveguide aperture spacing is made adjustable by using an optical bench as a track. The total
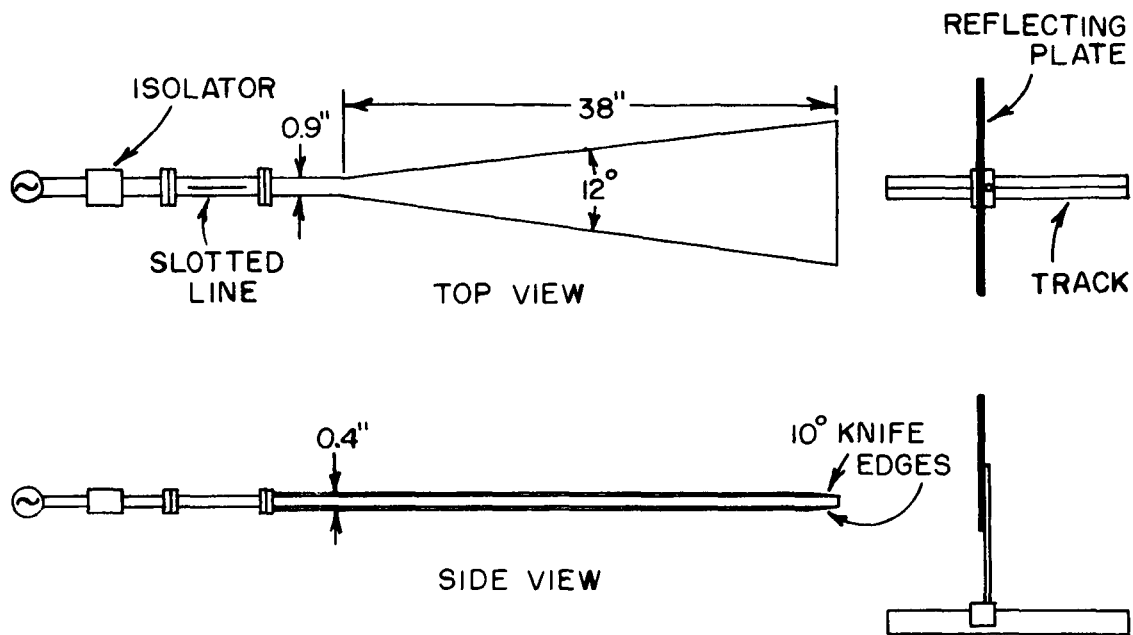
27

Fig. 14. Half-plane guide illuminating a reflecting
plate experimental apparatus.

reflection coefficient magnitude of the half-plane horn is measured

with a slotted line.

Reflection coefficient magnitude measurements were made

for the case of guide width (a) equal to 0.278λ and reflection plate

distance (r) in the range of $0.25\lambda < r < 2.3\lambda$. Comparisons between

calculated and measured reflection coefficient magnitudes are shown

in Fig. 15. It is to be noted that the apparent disagreement in the

curves (namely, a shift in (r) between the measured and calculated

curves) corresponds to an actual physical displacement of less than

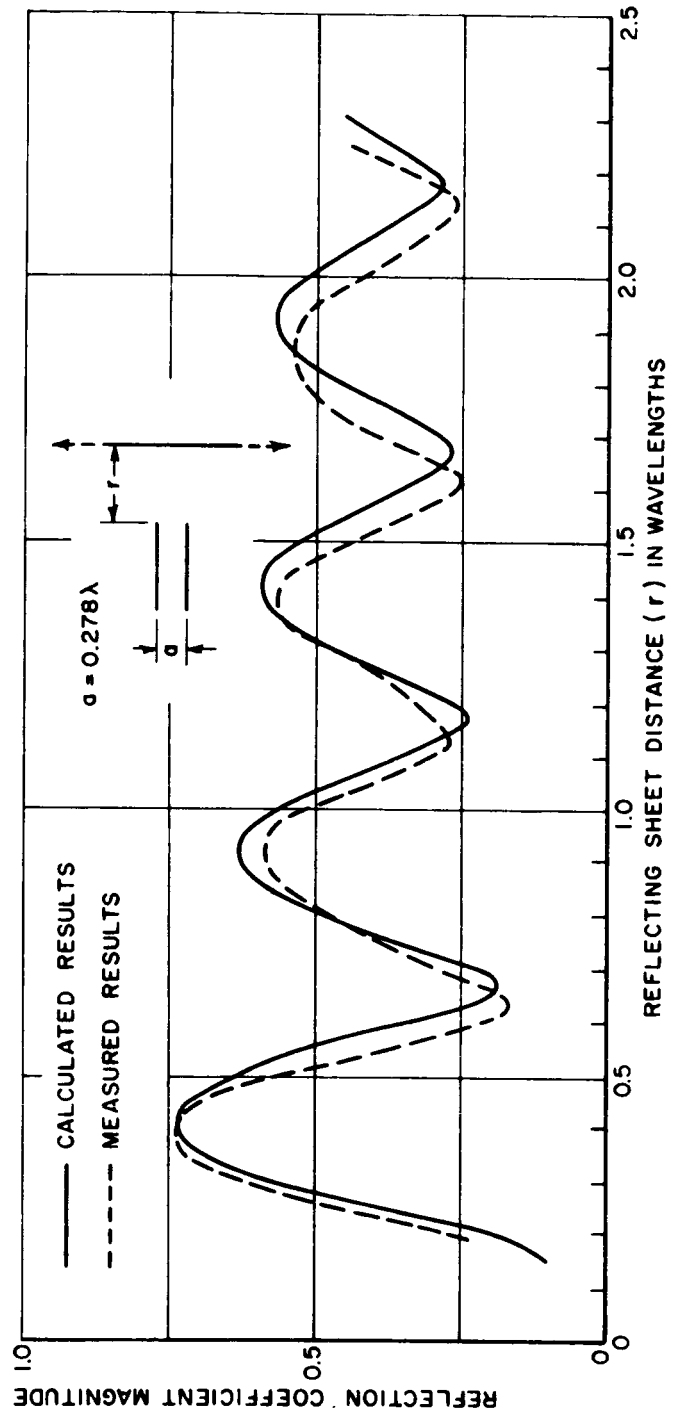2 mm and is well within experimental tolerances.

28

Fig. 15. Calculated vs. measured reflection coefficient magnitudes for a half-plane parallel plate waveguide illuminating a reflecting sheet.

29

CHAPTER IV
PLANE WAVE APPROACH FOR GUIDES WITH
FINITE WEDGE ANGLES LESS THAN 90°

A. Reflection Coefficient Analysis

By the analysis in Section IIA, the near-zone fields of a

normally truncated, symmetrical, TEM, parallel-plate wave-

guide are determined as basically those of a cylindrical wave.

For symmetrical guides with wedge angles significantly less than

90°, these near-fields may be approximated by plane waves in

the projected guide cross section. In this Chapter the reflection

coefficient is analyzed for a parallel-plate waveguide with wedge

angles less than 90° illuminating a conducting sheet by approxi-

mating the reflected field near the guide aperture by a plane wave.

The geometry of the problem is shown in Fig. 16. The guide is

composed of two wedges with equal wedge angles less than 90°.

The guide width is (a) and the separation between the conducting sheet

and the guide aperture is denoted as (r).

The situation depicted in Fig. 16 differs from that of Fig. 12

for the half-plane guide in the following way. Unlike the half-plane

guide case in which negligible diffraction occurs at the aperture for

the reflected (or image) wave, diffraction will occur at edges 1 and 2
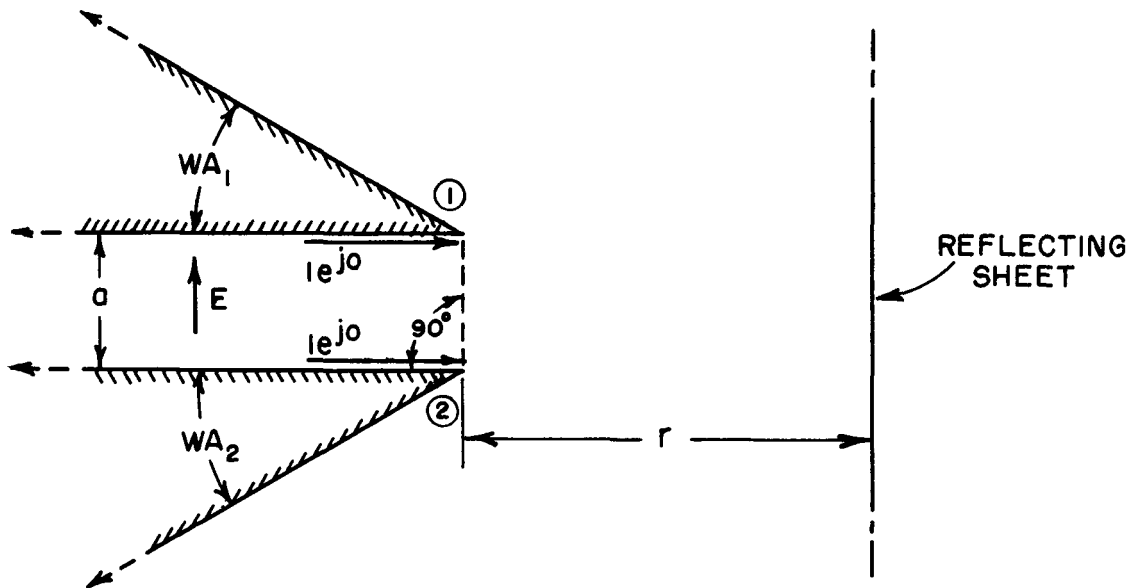
Fig. 16. Parallel-plate waveguide with WA < 90°
illuminating a reflecting sheet.

for this case. An outline of the analysis is as follows: The free

space wave of the guide that reflects off the reflecting sheet back

onto the guide aperture is denoted as the first-bounce wave or

reflection. The first-bounce wave in turn diffracts from the aperture

formed by the wedges, resulting in a second-bounce wave. The

second-bounce wave in turn reflects off the reflector back onto the

aperture, causing a third-bounce wave. This process continues

on indefinitely to higher-order bounces. In this analysis the wave

for each bounce is taken to be very nearly plane across the guide

aperture. Since the diffraction from the aperture of each incident

bounce wave depends only on the fields of the incident wave near the

aperture, each diffraction is treated as that of a plane wave. The

first-bounce wave caused by the initial guide radiation will be

analyzed first. Higher-order bounce waves will then be solved by

using the Higher-Order Diffraction Approach.[6,7]

1. First-bounce wave

As shown in Fig. 17, the first-bounce wave incident on the

guide aperture may be obtained by considering the free-space guide

magnetic field incident on the image guide located at a distance of

$2r$. $H_3^{(i)}$ and $H_4^{(i)}$ in Fig. 17b denote the magnetic fields incident

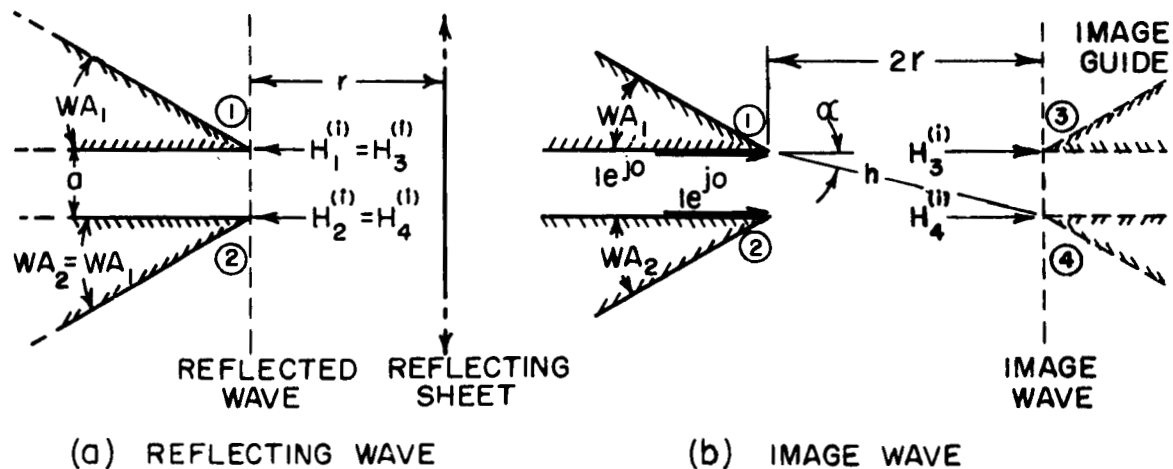(a) REFLECTING WAVE   (b) IMAGE WAVE

Fig. 17. First bounce reflected and equivalent
image wave.

on the image edges 3 and 4, respectively. The first-bounce fields incident on edges 1 and 2, $H_1^{(i)}$ and $H_2^{(i)}$ in Fig. 17a, are then exactly the same as the fields incident on the image edges in Fig. 17b. The slant distance from edge 1 to edge 4 and from edge 2 to edge 3 is denoted by (h) in Fig. 17b. The slant angle from 1 to 4 and 2 to 3 is denoted by (α) in the same figure.

The near-zone magnetic fields at the image edges ($H_3^{(i)}$ and $H_4^{(i)}$ in Fig. 17b) are accurately found by considering only the singly and doubly diffracted contributions from the transmitting guide. With unit amplitude magnetic fields inside the guide, the singly diffracted field contribution to $H_3^{(i)}$ from edge 1 is given by

$$(33) \qquad H_{13}^{(1)} = V_B(2r, \pi, n_1) \ ,$$

where n_1 is defined by $WA_1 = (2-n_1)\pi$. The subscript 13 denotes the field at edge 3 caused by the diffracted wave from edge 1. Similarly, the singly diffracted field component of $H_3^{(i)}$ from edge 2 is given by

$$(34) \qquad H_{23}^{(1)} = V_B(h, \pi - \alpha, n_2) \ .$$

The doubly diffracted field contribution to $H_3^{(i)}$ from edge 1 is caused by $R_2G^{(1)}$ (Eq. (11)) and is found, using Eqs. (5) and (18), to be

$$(35) \qquad H_{13}^{(2)} = R_2 G^{(1)} \times \frac{e^{-j\frac{\pi}{4}}}{\sqrt{2\pi k}} \times U_d$$

$$= \frac{\frac{1}{n_2} \sin \frac{\pi}{n_2}}{\cos \frac{\pi}{n_2} - \cos \frac{\pi/2}{n_2}}$$

$$\times \left[\frac{e^{-j\frac{\pi}{4}}}{\sqrt{2\pi k}} \times \frac{e^{-jk(a+2r)}}{\sqrt{a+2r}} \times e^{jk\frac{2ar}{a+2r}} \right]$$

$$\times \left[V_B\left(\frac{2ar}{a+2r}, \frac{\pi}{2}, n_1\right) + V_B\left(\frac{2ar}{a+2r}, \frac{3\pi}{2}, n_1\right) \right] .$$

The doubly diffracted contribution to $H_3^{(i)}$ from edge 2 is given similarly by

$$(36) \qquad H_{23}^{(2)} = R_1 G^{(1)} \times \frac{e^{-j\frac{\pi}{4}}}{\sqrt{2\pi k}} \times U_d$$

$$= \frac{\frac{1}{n_1} \sin \frac{\pi}{n_1}}{\cos \frac{\pi}{n_1} - \cos \frac{\pi/2}{n_1}}$$

$$\cdot \left[\frac{e^{-j\frac{\pi}{4}}}{\sqrt{2\pi k}} \times \frac{e^{-jk(a+h)}}{\sqrt{a+h}} \times e^{jk\frac{ah}{a+h}} \right]$$

$$\times \left[V_B\left(\frac{ah}{a+h}, \frac{\pi}{2} - \alpha, n_2\right) + V_B\left(\frac{ah}{a+h}, \frac{3\pi}{2} - \alpha, n_2\right) \right] .$$

$H_3^{(i)}$ is then given by

$$(37) \qquad H_3^{(i)} = H_{13}^{(1)} + H_{13}^{(2)} + H_{23}^{(1)} + H_{23}^{(2)} \qquad .$$

$H_4^{(i)}$ may be obtained similarly. The singly diffracted field components of $H_4^{(i)}$ are

$$(38) \qquad H_{14}^{(1)} = V_B(h, \pi - \alpha, n_1)$$

and

$$(39) \qquad H_{24}^{(1)} = V_B(2r, \pi, n_2) \ .$$

The doubly diffracted field contributions are

$$(40) \qquad H_{14}^{(2)} = R_2 G^{(1)} \times \frac{e^{-j\frac{\pi}{4}}}{\sqrt{2\pi k}} \times U_d$$

$$= \frac{\frac{1}{n_2} \sin \frac{\pi}{n_2}}{\cos \frac{\pi}{n_2} - \cos \frac{\pi/2}{n_2}}$$

$$\times \left[\frac{e^{-j\frac{\pi}{4}}}{\sqrt{2\pi k}} \times \frac{e^{-jk(a+h)}}{\sqrt{a+h}} \times e^{jk\frac{ah}{a+h}} \right]$$

$$\times \left[V_B \left(\frac{ah}{a+h}, \frac{\pi}{2} - \alpha, n_1 \right) + V_B \left(\frac{ah}{a+h}, \frac{3\pi}{2} - \alpha, n_1 \right) \right] \qquad ,$$

and

$$(41) \quad H_{24}^{(2)} = R_1 G^{(1)} \times \frac{e^{-j\frac{\pi}{4}}}{\sqrt{2\pi k}} \times U_d$$

$$= \frac{\frac{1}{n_1} \sin \frac{\pi}{n_1}}{\cos \frac{\pi}{n_1} - \cos \frac{\pi/2}{n_1}}$$

$$\times \left[\frac{e^{-j\frac{\pi}{4}}}{\sqrt{2\pi k}} \times \frac{e^{-jk(a+2r)}}{\sqrt{a+2r}} \times e^{jk\frac{2ar}{a+2r}} \right]$$

$$\times \left[V_B \left(\frac{2ar}{a+2r}, \frac{\pi}{2}, n_2 \right) + V_B \left(\frac{2ar}{a+2r}, \frac{3\pi}{2}, n_2 \right) \right]$$

$H_4^{(i)}$ is then given by

$$(42) \quad H_4^{(i)} = H_{14}^{(1)} + H_{14}^{(2)} + H_{24}^{(1)} + H_{24}^{(2)}$$

The first-bounce fields reflected back onto edges 1 and 2 by the reflecting sheet, $H_1^{(i)}$ and $H_2^{(i)}$ in Fig. 17a, are then obtained from Eqs. (37) and (42) by the following equivalence:

$$(43) \quad H_1^{(i)} = H_3^{(i)}$$

$$H_2^{(i)} = H_4^{(i)}$$

2. Higher-order bounce wave

The first-bounce wave diffracts from the aperture of the guide forming a second-bounce wave. This second-bounce wave reflects

from the reflecting sheet back onto the guide aperture causing a third-bounce wave. The continuation of this process then results in the formation of all higher-order bounce waves. Since the wave for each bounce is nearly plane, each bounce-wave diffraction may be treated as that of a plane wave.

In this analysis, the contribution of all subsequent bounce waves other than the first bounce is thought of as that of the higher-order bounce wave. The fields of this higher-order bounce wave are obtained through use of the "self-consistency" principle in the Higher-Order Diffraction Method.

The total fields incident on edges 1 and 2 due to all the bounce waves are denoted by H_1 and H_2 respectively with

$$(44) \qquad H_1 = H_1{}^{(i)} + H_1{}^{(h)},$$

and

$$(45) \qquad H_2 = H_2{}^{(i)} + H_2{}^{(h)},$$

where $H_1{}^{(h)}$ and $H_2{}^{(h)}$ are the higher-order bounce fields incident on the guide edges. H_1, H_2, $H_1{}^{(h)}$, and $H_2{}^{(h)}$ in Eqs. (44) and (45) are, of course, still unknown. H_1 and H_2 incident on edges 1 and 2 cause the higher-order bounce fields $H_3{}^{(h)}$ and $H_4{}^{(h)}$ to be incident on the image edges 3 and 4 as shown in Fig. 18. But by image theory the field incident on the image edges are precisely those incident on

37
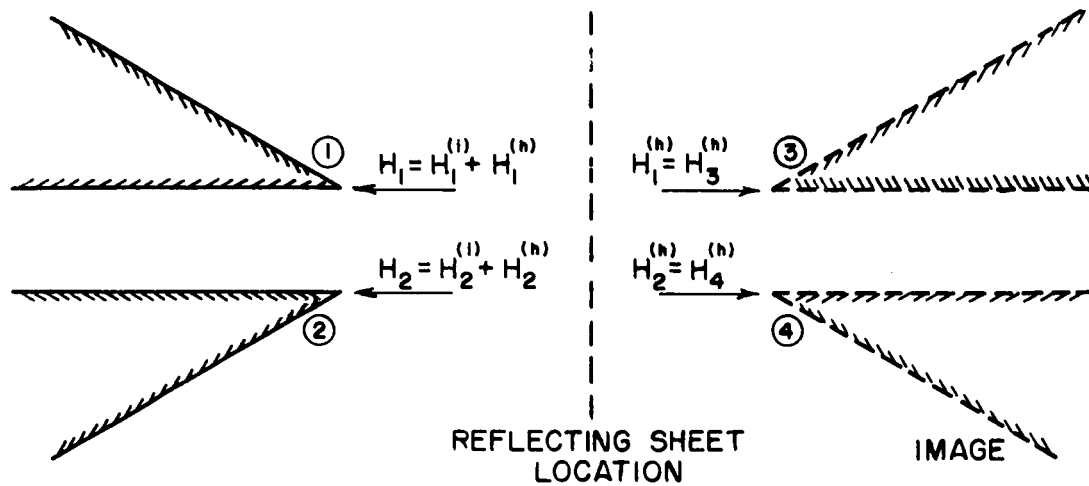
Fig. 18. Higher-order bounce fields incident
on the guide edges.

the guide edges. Hence the higher-order bounce wave fields incident

on edges 1 and 2 are given by

$$(46) \qquad H_1{}^{(h)} = H_3{}^{(h)} \; ,$$

and

$$(47) \qquad H_2{}^{(h)} = H_4{}^{(h)}$$

where $H_3{}^{(h)}$ and $H_4{}^{(h)}$ are still unknown.

H_1 and H_2 incident on edges 1 and 2, respectively, also cause

the rays $R_1G^{(r)}$ and $R_2G^{(r)}$ to propagate in the directions of the cor-

respondingly opposite edges as shown in Fig. 19. The superscripts

$WA_1 = (2 - n_1)\pi$

a

$R_1^{(r)}$

$R_{1G}^{(r)}$

H_1

$R_2^{(r)}$

$R_{2G}^{(r)}$

H_2

$WA_2 = (2 - n_2)\pi$
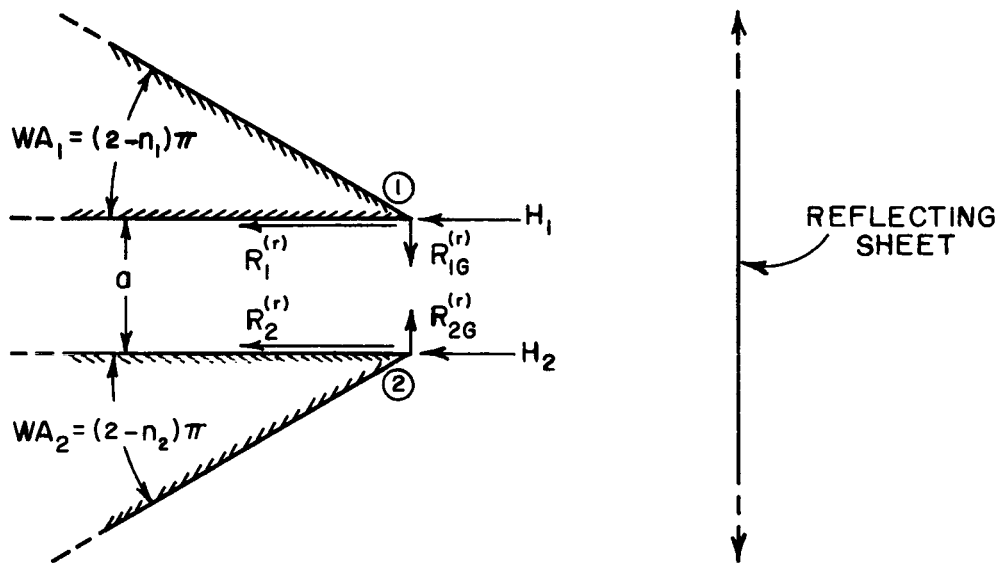
REFLECTING
SHEET

Fig. 19. Effect of the total reflected wave
incident on the guide aperture.

(r) indicate that $R_{1G}^{(r)}$ and $R_{2G}^{(r)}$ are caused by reflection at the

reflecting sheet. These rays are respectively given by

$$(48) \qquad R_{1G}^{(r)} = H_1 \left[\frac{\dfrac{1}{n_1} \sin \dfrac{\pi}{n_1}}{\cos \dfrac{\pi}{n_1} - \cos \dfrac{-\pi/2}{n_1}} + \frac{\dfrac{1}{n_1} \sin \dfrac{\pi}{n_1}}{\cos \dfrac{\pi}{n_1} - \cos \dfrac{3\pi/2}{n_1}} \right] ,$$

and

$$(49) \qquad R_{2G}^{(r)} = H_2 \left[\frac{\dfrac{1}{n_2} \sin \dfrac{\pi}{n_2}}{\cos \dfrac{\pi}{n_2} - \cos \dfrac{-\pi/2}{n_2}} + \frac{\dfrac{1}{n_2} \sin \dfrac{\pi}{n_2}}{\cos \dfrac{\pi}{n_2} - \cos \dfrac{3\pi/2}{n_2}} \right] .$$

39

Applying the Higher-Order Diffraction Method, H_1, the total magnetic field incident on edge 1 due to reflection by the reflecting sheet, is given by

(50)
$$H_1 = H_1^{(i)} + H_1^{(h)}$$

$$= H_1^{(i)} + R_2 G^{(r)} \left[\frac{e^{-j\frac{\pi}{4}}}{\sqrt{2\pi k}} \quad \frac{e^{-jk(a+2r)}}{\sqrt{a+2r}} \quad e^{jk\frac{2ar}{a+2r}} \right]$$

$$\times \left[V_B\left(\frac{2ar}{a+2r}, \frac{\pi}{2}, n_1 \right) + V_B\left(\frac{2ar}{a+2r}, \frac{3\pi}{2}, n_1 \right) \right]$$

$$+ H_1 \times \left[V_B(2r, 0, n_1) + V_B(2r, 2\pi, n_1) \right]$$

$$+ H_2 \times \left[V_B(h, -\alpha, n_2) + V_B(h, 2\pi - \alpha, n_2) \right]$$

$$+ R_1 G^{(r)} \times \left[\frac{e^{-j\frac{\pi}{4}}}{\sqrt{2\pi k}} \quad \frac{e^{-jk(a+h)}}{\sqrt{a+h}} \quad e^{jk\frac{ah}{a+h}} \right]$$

$$\times \left[V_B\left(\frac{ah}{a+h}, \frac{\pi}{2} - \alpha, n_2 \right) + V_B\left(\frac{ah}{a+h}, \frac{3\pi}{2} - \alpha, n_2 \right) \right] \quad .$$

H_2, the total magnetic field incident on edge 2 from outside the guide is similarly given by

40

(51) $\qquad H_2 = H_2{}^{(i)} + H_2{}^{(h)}$

$$= H_2{}^{(i)} + R_1G{}^{(r)} \left[\frac{e^{-j\frac{\pi}{4}}}{\sqrt{2\pi k}} \quad \frac{e^{-jk(a+2r)}}{\sqrt{a+2r}} \quad e^{jk\frac{2ar}{a+2r}} \right]$$

$$\times \left[V_B\left(\frac{2ar}{a+2r}, \frac{\pi}{2}, n_2\right) + V_B\left(\frac{2ar}{a+2r}, \frac{3\pi}{2}, n_2\right) \right]$$

$$+ H_2 \times \left[V_B(2r, 0, n_2) + V_B(2r, 2\pi, n_2) \right]$$

$$+ H_1 \times \left[V_B(h, -\alpha, n_1) + V_B(h, 2\pi-\alpha, n_1) \right]$$

$$+ R_2G{}^{(r)} \times \left[\frac{e^{-j\frac{\pi}{4}}}{\sqrt{2\pi k}} \quad \frac{e^{-jk(a+h)}}{\sqrt{a+h}} \quad e^{jk\frac{ah}{a+h}} \right]$$

$$\times \left[V_B\left(\frac{ah}{a+h}, \frac{\pi}{2} - \alpha, n_1\right) + V_B\left(\frac{ah}{a+h}, \frac{3\pi}{2} - \alpha, n_1\right) \right] \qquad .$$

Solving Eqs. (50) and (51) simultaneously with the parametric Eqs. (48) and (49), H_1 and H_2 may be obtained. $R_1G{}^{(r)}$ and $R_2G{}^{(r)}$ are then obtained from Eqs. (48) and (49).

The contributions of H_1 and H_2 to the reflection coefficient are computed by considering the rays $R_1{}^{(r)}$ and $R_2{}^{(r)}$ propagating back into the guide from the edges as shown in Fig. 19. $R_1{}^{(r)}$ and $R_2{}^{(r)}$ represent the total rays from edges 1 and 2, respectively, propagating

41

back into the waveguide due to the reflection by the conducting sheet
and are given by

$$(52) \qquad R_1^{(r)} = H_1 \left[e^{j \frac{\pi}{4}} \sqrt{2 \pi k} \right]$$

$$+ R_2 G^{(r)} \times \left[V_B \left(a, -\frac{\pi}{2}, n_1 \right) + V_B \left(a, \frac{\pi}{2}, n_1 \right) \right] \quad ,$$

and

$$(53) \qquad R_2^{(r)} = H_2 \left[e^{j \frac{\pi}{4}} \sqrt{2 \pi k} \right]$$

$$+ R_1 G^{(r)} \times \left[V_B \left(a, -\frac{\pi}{2}, n_2 \right) + V_B \left(a, \frac{\pi}{2}, n_2 \right) \right] \quad .$$

The reflection coefficient of the waveguide due to the conductor-
sheet reflection is then given by

$$(54) \qquad \Gamma_r = \frac{1}{2} \sqrt{\frac{\lambda}{2 \pi k a}} \left[R_1^{(r)} + R_2^{(r)} \right] e^{-j \frac{\pi}{2}} \quad .$$

The total reflection coefficient Γ_T is obtained by summing the
guide self reflection coefficient Γ_0 given by Eq. (30) and the reflection
coefficient Γ_r due to the reflecting sheet as given by Eq. (54). Thus

$$(55) \qquad \Gamma_T = \Gamma_0 + \Gamma_r \quad .$$

B. Results

The reflection coefficients of symmetrical guides with wedge

angles less than 90° illuminating a reflecting sheet were calculated

by the "plane wave approach" with the aid of a Scatran program on

an IBM 7094 digital computer. A statement listing for the V_B sub-

routine used may be found in Reference [7].

Measurement of the total reflection coefficient was made with

essentially the same experimental apparatus as shown in Fig. 14

except that conducting plates were attached to the sectoral horn

aperture to simulate conducting wedges. Calculated and measured

total reflection coefficient magnitudes are presented in Figs. 20

and 21. Figure 20 shows the result for a TEM parallel-plate

waveguide of 0.278λ guide width with 60° wedges. Figure 21 shows

the result for the same guide with 75° wedges. Besides the total

reflection coefficient magnitudes calculated by the "plane wave

higher order" method in this chapter, Figs. 20 and 21 also show

the reflection coefficient magnitudes for the same guides not

including the higher-order bounces. It should be noted that although

seemingly good agreement is achieved between theoretical and

measured results by the method outlined in this section, the verifi-

cation cannot be termed conclusive because the "plane wave reflection"

higher-order contributions are small compared to the single bounce

reflection coefficient.

Figure 22 presents the phase of the total reflection coefficient for the guide with 75° wedge angles and 0.278λ guide width. The calculated Γ_T magnitude for a guide of 0.7λ guide width and 75° wedge angle is shown in Figs. 23 and 24.
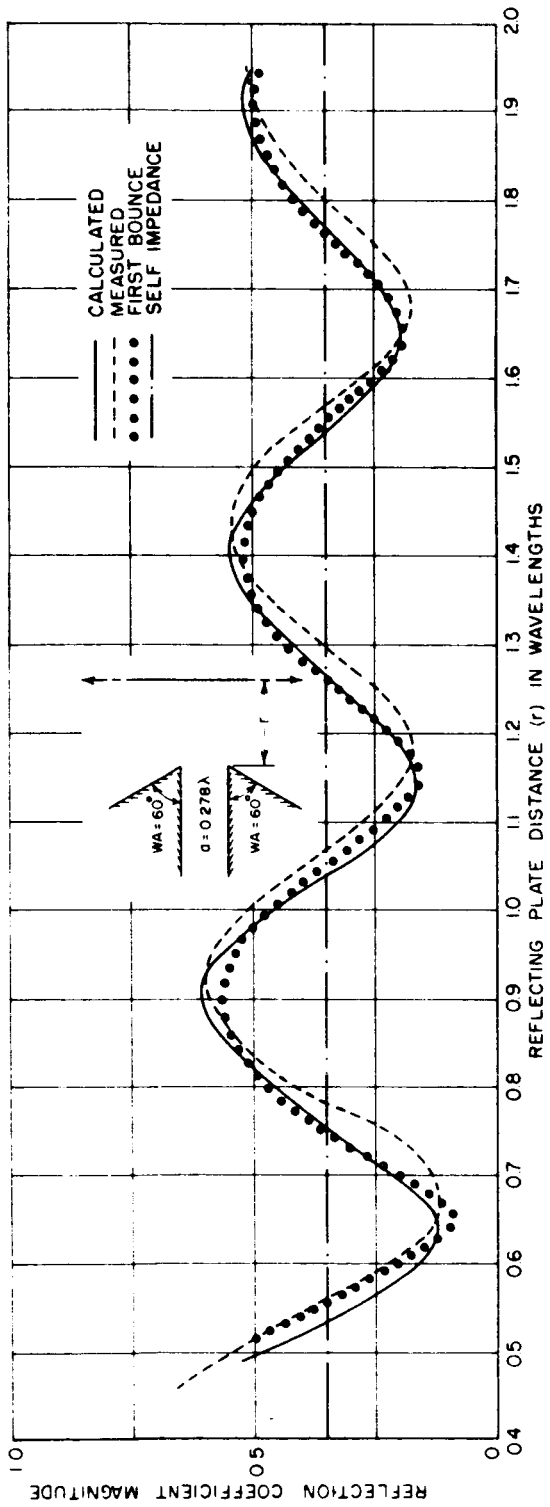
Fig. 20. Reflection coefficient magnitude for a TEM guide with 60° wedge angles illuminating a reflecting sheet.

45

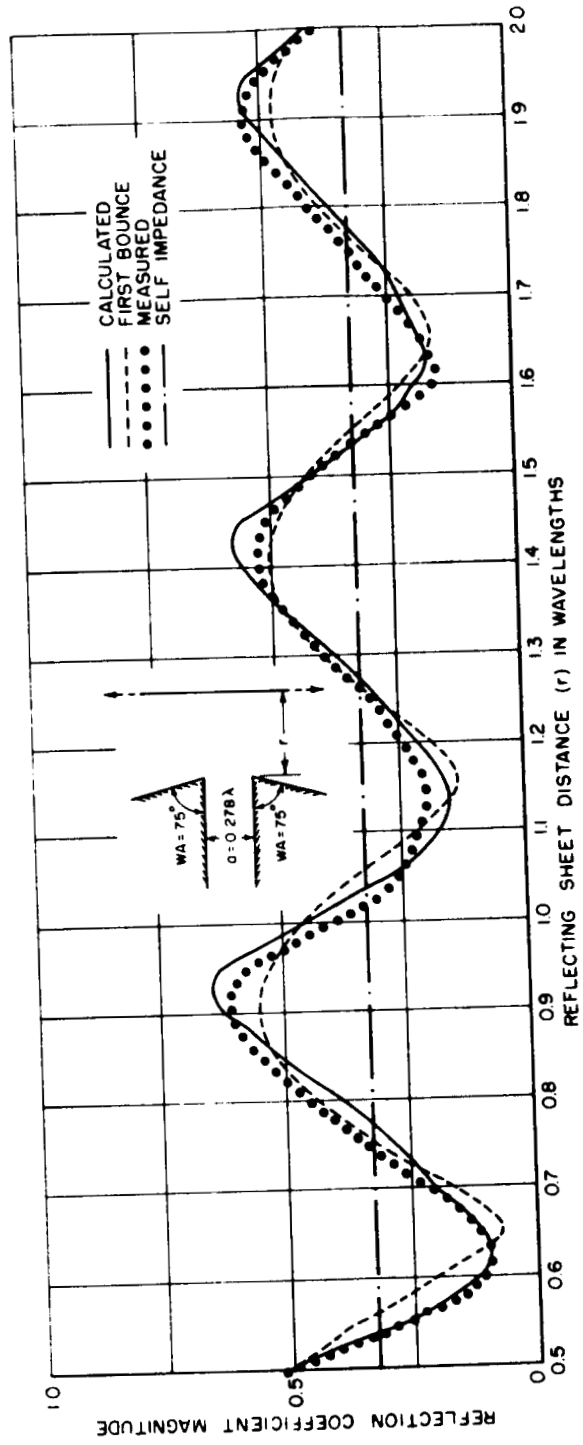Fig. 21. Reflection coefficient magnitude for a TEM guide with WA = 75° illuminating a reflecting sheet.

46
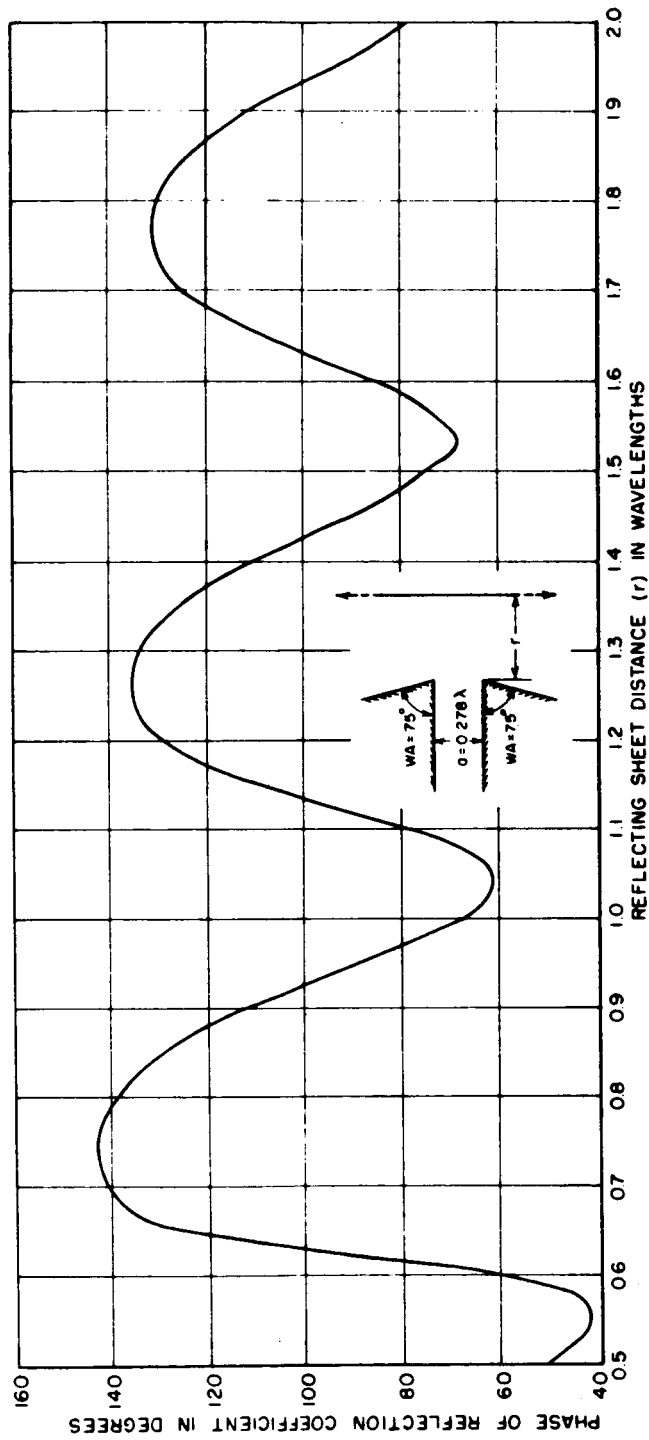
Fig. 22. Reflection coefficient phase for a TEM guide (WA = 75°, a = 0.278λ) illuminating a reflecting sheet.

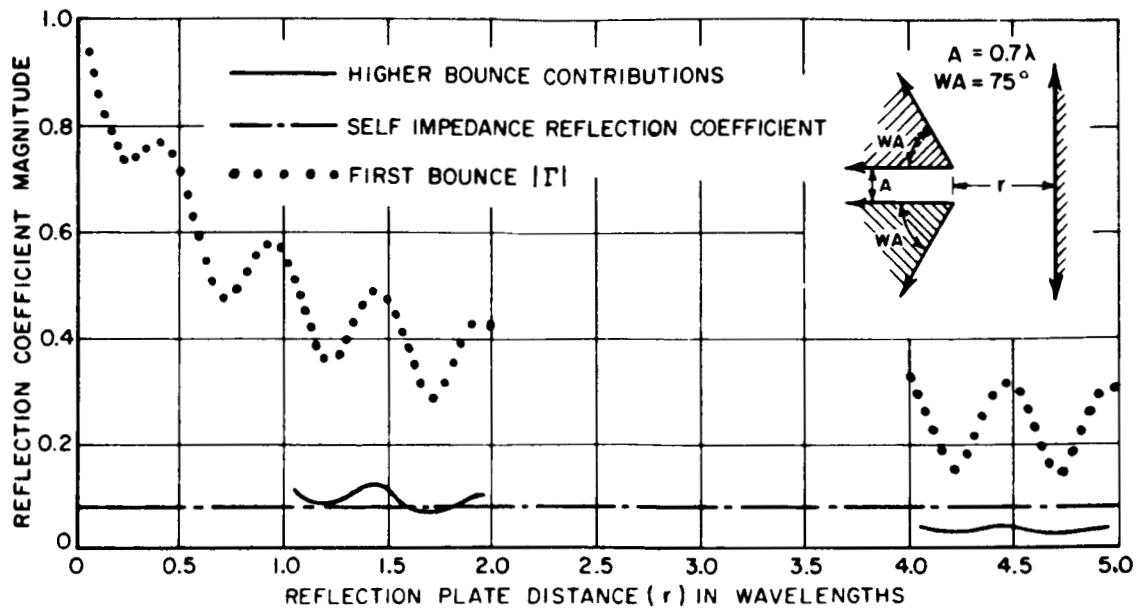Fig. 23. First bounce reflection coefficient magnitude
for a TEM guide with 75° wedge angles illumi-
nating a reflecting sheet.
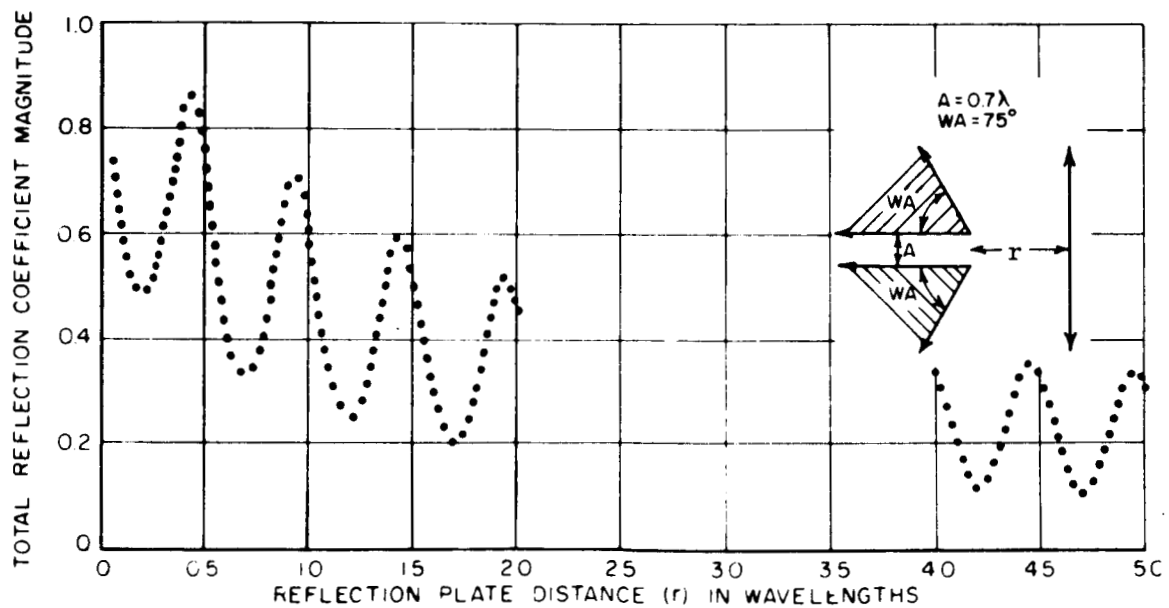
Fig. 24. Reflection coefficient magnitude for a TEM guide
with 75° wedge angles illuminating a reflecting
sheet.

48

CHAPTER V
CYLINDRICAL BOUNCE WAVE APPROACH FOR
GROUND-PLANE MOUNTED GUIDES

A. Reflection Coefficient Analysis

The problem of analyzing the reflection coefficient of a TEM

parallel-plate waveguide mounted in a ground-plane and illuminating

a perfectly reflecting sheet perpendicular to the guide axis is

treated in this section. The geometry of the problem is as shown

in Fig. 25.

Fig. 25. Ground-plane mounted parallel-plate waveguide
illuminating a reflecting sheet.

For this problem, the plane wave analysis of Chapter IV is not

valid because the reflected wave fields from the reflecting sheet

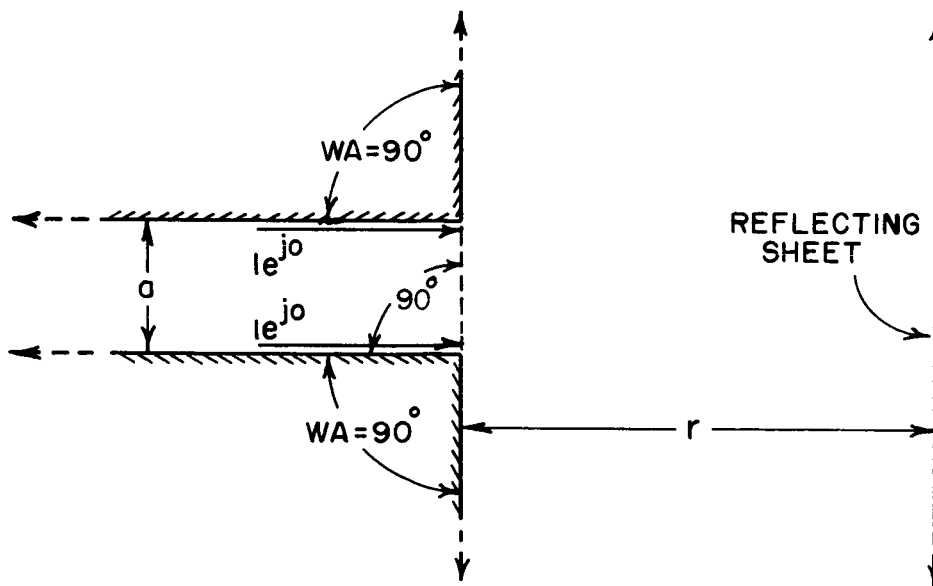incident on the guide have reflection boundaries from the wedges as

shown in Fig. 26. The diffracted wave depends on the incident wave
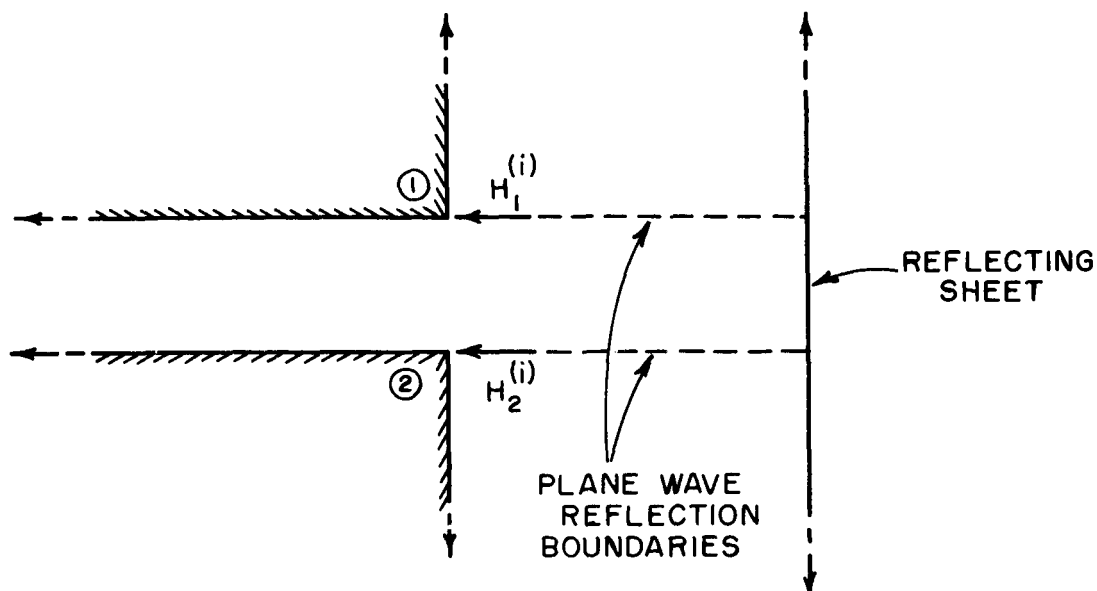
Fig. 26. Reflection boundaries for the plane reflection
waves predicted by Chapter IV.

over a wide region near the shadow boundaries. The first-bounce

wavefront incident on the guide, represented by $H_1^{(i)}$ and $H_2^{(i)}$, is

actually cylindrical but assumed plane to a good approximation in the

analysis of Chapter IV. The assumption that the diffracted fields

caused by the first-bounce wave are accurately given by plane wave

diffraction is not valid near the shadow boundaries of the incident

wave. For this problem the exact nature of each bounce wave is

taken into account in an iterative method of "successively bouncing cylindrical waves."

An outline of the analysis is as follows: The magnetic field plot for the ground-plane mounted guide obtained by the method given in Section IIA indicates that the field of the guide in the near zone is cylindrical. This cylindrical magnetic field plot, taken at a distance (2r) from the guide aperture, represents the reflected wave from the conducting sheet, located at a distance (r) from the aperture, incident on the ground-plane mounted guide aperture. This reflected wave is called the first-bounce wave. Because the first-bounce wave is cylindrical, an equivalent line source is introduced to compute the first-bounce wave contribution to the reflection coefficient by the line source to waveguide coupling expression in Section IIB.

The first-bounce wave, incident on the guide aperture in the ground-plane, causes a second-bounce wave. In view of the cylindrical nature of the first-bounce wave, the second-bounce diffracted wave can be treated as the result of the diffraction of a cylindrical wave from the ground-plane mounted guide aperture. Unlike the first-bounce wave, the second-bounce wave is not cylindrical. However, by referring to Fig. 29, it appears that the nature of the second-bounce wave may be represented in terms of the superposition of two cylindrical waves: the geometrical optics

component of the first-bounce wave, and the diffracted wave of the first-bounce wave by a rectangular wall. Thus the second-bounce wave has been separated into these two components which were indeed found to be close to cylindrical waves. Since it can be assumed that two cylindrical components result for the second bounce wave, two equivalent line sources and hence two reflection coefficient components will result for the second-bounce wave.

Like the first-bounce wave, the two cylindrical components of the second-bounce wave will each cause two diffracted cylindrical components which constitute the third-bounce wave. The four cylindrical components of the third-bounce wave then require four equivalent line sources to compute the third-bounce reflection coefficient contribution. The same relationship applies to successive bounce waves. More specifically, the fourth-bounce wave will have eight components and the fifth-bounce wave sixteen components.

1. First-bounce wave

The geometry for the equivalent line source determination is shown in Fig. 27 for the first-bounce wave (the initial guide wave reflected by the reflecting sheet). Figure 27 depicts the first-bounce wavefront incident on the guide with a cylindrical phase contour. An equivalent line source located at a distance $\rho^{(1)}$ from the guide will generate this phase front if
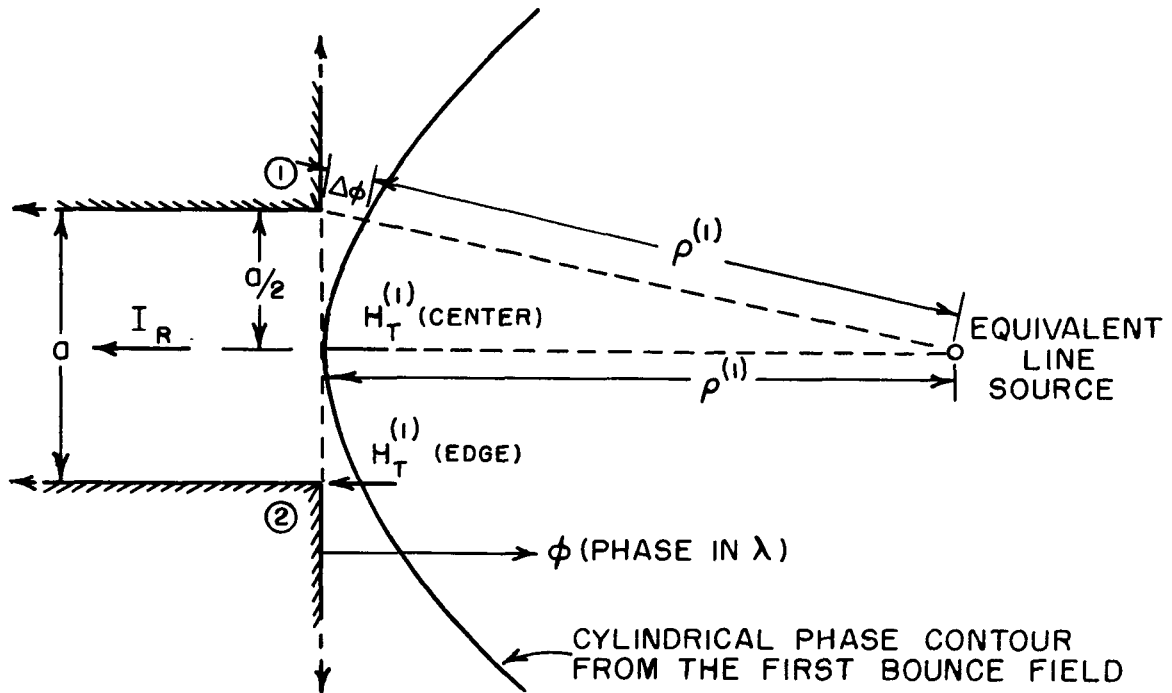
Fig. 27. Equivalent line source determination
for the first-bounce fields.

$$(56) \qquad \rho^{(1)} = \frac{a^2}{8\Delta\phi} - \frac{\Delta\phi}{2} \; ,$$

where $\Delta\phi$ is the phase difference expressed in wavelengths between

the first-bounce magnetic fields at the center of the guide aperture,

$H_T^{(1)}$ (center), and at one of the guide edges, $H_T^{(1)}$ (edge). Super-

scripts denote the bounce number in this chapter. The modal current

of the equivalent line source is related to the first-bounce magnetic

field at the center of the guide aperture by Eq. (18) and is given by

$$(57) \qquad I_{eq}{}^{(1)} = \sqrt{2\pi\rho^{(1)}} \ e^{jk\rho^{(1)} - j\frac{\pi}{4}} \ H_T{}^{(1)} \ (\text{center}),$$

where $H_T{}^{(1)}$ (center), the magnetic field at the center of the guide aperture, is computed by Eq. (17).

The power flowing back into the guide caused by the first-bounce wave may be related to the first-bounce equivalent line source current, $I_{eq}{}^{(1)}$ of Eq. (57), by Eq. (21) and expressed in terms of the modal current in the guide. Line source to waveguide coupling yields the guide modal current as

$$(58) \qquad I_R{}^{(1)} = I_{eq}{}^{(1)} \sqrt{\frac{\lambda}{2\pi a}} \ \ H_T \ (\rho^{(1)}) \ .$$

$H_T \ (\rho^{(1)})$ is computed by Eq. (17) for the field point along the guide axis at the distance of $\rho^{(1)}$ with the guide transmitting a modal current equal to $\sqrt{a}$. The contribution to the reflection coefficient by the first-bounce wave is thus given by

$$(59) \qquad \Gamma^{(1)} = \frac{I_R{}^{(1)}}{I_o} = \frac{I_R{}^{(1)}}{\sqrt{a}}$$

$$= \frac{I_{eq}{}^{(1)}}{a} \ \sqrt{\frac{\lambda}{2\pi}} \ \ H_T(\rho^{(1)}) \ .$$

2. Second-bounce wave

The first-bounce wave incident on the waveguide aperture causes a second-bounce wave that is mainly composed of the reflected

54

geometrical optics field and to a lesser extent the other cylindrical wave component which is analogous to the diffracted wave from a rectangular wall. The second-bounce wave is reflected from the reflecting sheet back onto the guide aperture. The fields of the second-bounce wave incident on the guide aperture are, of course, given by image theory as the fields of this wave at a distance $(2r)$ from the guide aperture. The geometry for the second-bounce wave field plot is as shown in Fig. 28. The distances to the field point $P(x, y)$ from edges 1 and 2 are denoted by r_1 and r_2, respectively. The distance from the line source to either edge is denoted by $\tau^{(1)}$.

The second-bounce fields along the field plot plane may then be obtained by again considering only the singly and doubly diffracted contributions. Singly diffracted contributions are given by the diffraction of the cylindrical wave of the equivalent line source by the individual wedges. The singly diffracted magnetic field at $P(x, y)$ from edge 1 is obtained from Eqs. (5) and (18) and is given by
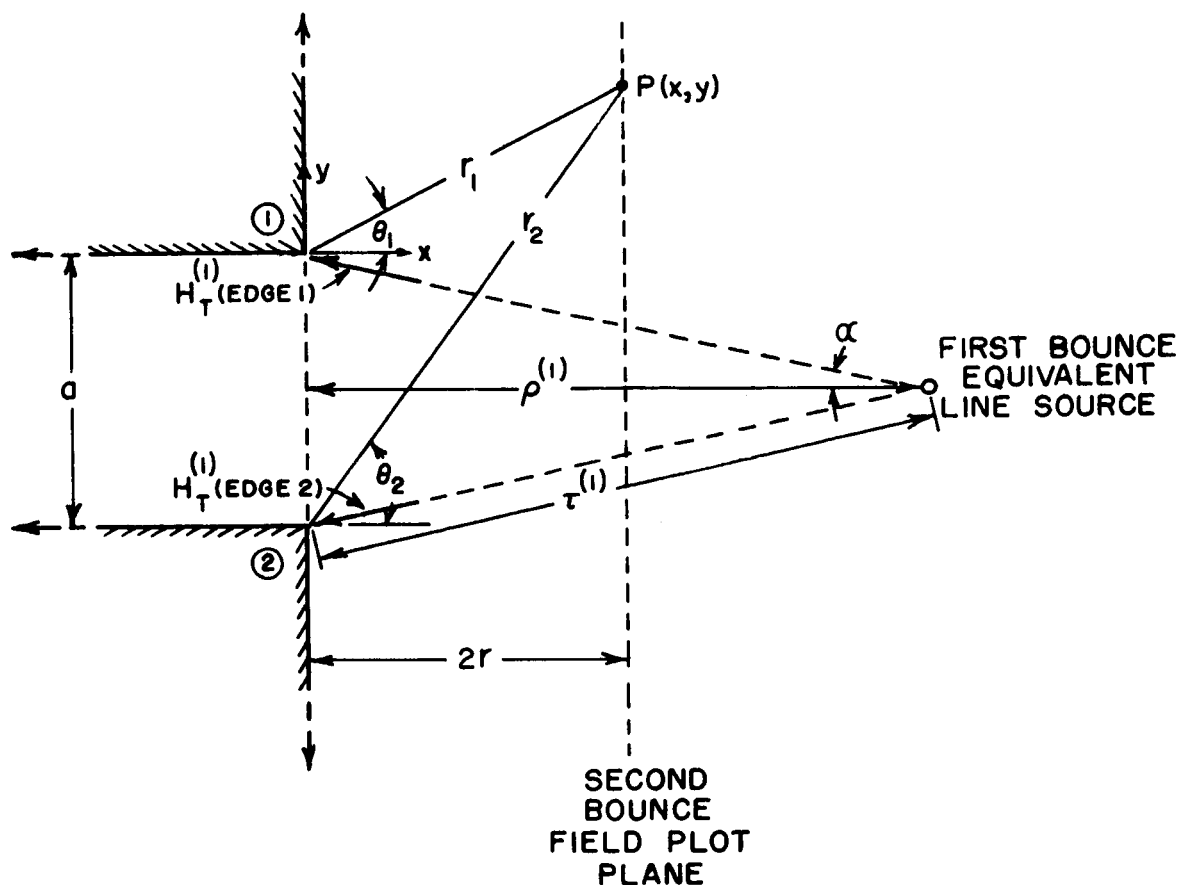
Fig. 28. Second-bounce field plot geometry.

$$(60) \qquad \text{HD}_1{}^{(1)}(P) = \sqrt{\tau^{(1)}} \; e^{jk\tau^{(1)}} \; \text{H}_T{}^{(1)} \quad (\text{edge 1})$$

$$\times \left\{ \frac{e^{jk\left[\dfrac{r_1 \cdot \tau^{(1)}}{r_1 + \tau^{(1)}} - (r_1 + \tau^{(1)})\right]}}{\sqrt{r_1 + \tau^{(1)}}} \right\}$$

$$\times \left[V_B \left(\frac{r_1 \cdot \tau^{(1)}}{r_1 + \tau^{(1)}}, \; \theta_1 + \alpha, \; n_1 \right) \right.$$

$$\left. + \quad V_B \left(\frac{r_1 \cdot \tau^{(1)}}{r_1 + \tau^{(1)}}, \; 2\pi + \theta_1 - \alpha, \; n_1 \right) \right] \;.$$

Similarly the singly diffracted field from edge 2 is given by

$$(61) \qquad HD_2^{(1)}(P) = \sqrt{\tau^{(1)}} \, e^{jk\tau^{(1)}} \, HT^{(1)} \quad \text{(edge 2)}$$

$$\times \left\{ \frac{e^{jk\left[\frac{r_2 \cdot \tau^{(1)}}{r_2 + \tau^{(1)}} - (r_2 + \tau^{(1)})\right]}}{\sqrt{r_2 + \tau^{(1)}}} \right\}$$

$$\times \left[V_B \left(\frac{r_2 \, \tau^{(1)}}{r_2 + \tau^{(1)}}, \, \alpha - \theta_2, \, n_2 \right) \right.$$

$$\left. + V_B \left(\frac{r_2 \, \tau^{(1)}}{r_2 + \tau^{(1)}}, \, 2\pi - \theta_2 - \alpha, \, n_2 \right) \right] \quad .$$

The doubly diffracted fields are caused by the singly diffracted waves from the edges diffracting off their correspondingly opposite edges. Because the singly diffracted waves in their directions of interest are removed from shadow boundaries they may be treated as cylindrical waves. Consequently the line source diffraction formulation of Eq. (5) is used to give the doubly diffracted fields. The doubly diffracted field from edge 1 is given by

$$(62) \quad H_{DD1}^{(2)}(P) = D_{D2}G^{(1)}$$

$$\times \left[V_B\left(\frac{a \cdot r_1}{r_1 + a}, \frac{\pi}{2} + \theta_1, n_1\right)\right.$$

$$+ \left. V_B\left(\frac{a \cdot r_1}{r_1 + a}, \frac{3\pi}{2} + \theta_1, n_1\right)\right]$$

$$\times \left\{ \frac{e^{jk\left[\frac{a \cdot r_1}{a + r_1} - (r_1 + a)\right]}}{\sqrt{r_1 + a}} \right\} \quad ,$$

where

$$(63) \quad D_{D2}G^{(1)} = \sqrt{\tau^{(1)}} \, e^{jk\tau^{(1)}} H_T^{(1)} \text{ (edge 2)}$$

$$\times \left[V_B\left(\tau^{(1)}, \alpha - \frac{\pi}{2}, n_2\right) + V_B\left(\tau^{(1)}, \frac{3\pi}{2} - \alpha, n_2\right)\right] .$$

$D_{D2}G^{(1)}$ denotes the diffraction coefficient of the ray from edge 2 to edge 1 caused by the incidence of $H_T^{(1)}$ (edge 2) on edge 2. Similarly the doubly diffracted magnetic field at $P(x, y)$ from edge 2 is given by

$$(64) \quad H_{DD2}^{(2)}(P) = D_{D1}G^{(1)}$$

$$\times \left[V_B\left(\frac{a \cdot r_2}{a + r_2}, \frac{\pi}{2} - \theta_2, n_2\right)\right.$$

$$+ \left. V_B\left(\frac{a \cdot r_2}{a + r_2}, \frac{3\pi}{2} - \theta_2, n_2\right)\right]$$

$$\times \left\{ \frac{e^{jk\left[\frac{a \cdot r_2}{a + r_2} - (a + r_2)\right]}}{\sqrt{a + r_2}} \right\} \quad ,$$

58

where

(65) $DD_1G^{(1)} = \overline{\sqrt{\tau^{(1)}}} \; e^{jk\tau^{(1)}} \; H_T^{(1)}$ (edge 1)

$$\times \left[V_B \left(\tau^{(1)}, \alpha - \frac{\pi}{2}, n_1 \right) + V_B \left(\tau^{(1)}, \frac{3\pi}{2} - \alpha, n_1 \right) \right] \quad .$$

The total field at P(x, y) is given by

(66) $H_T^{(2)}(P) = H_{D1}^{(2)}(P) + H_{DD_1}^{(2)}(P) + H_{D2}^{(2)}(P) + H_{DD_2}^{(2)}(P)$

$$+ \left\{ \begin{array}{ll} I_{eq}^{(1)} \; \dfrac{e^{-jk\rho' + j\frac{\pi}{4}}}{\sqrt{2\pi\rho'}} & \text{for } \theta_1 \geq \alpha \text{ or } \theta_1 \leq \alpha \\ \\ 0 & \text{otherwise} \end{array} \right\} ,$$

where the bracketed term is the reflected geometrical optics field from the ground-plane guide aperture. It is to be noted that $H_T^{(2)}(P)$ describes the second-bounce field plot as P varies.

The second-bounce wave field plot according to Eq. (66) does not have a cylindrical wavefront like the first-bounce wave. Consequently a single equivalent line source will not suffice to describe its wavefront. Superposition is used to accurately describe the second-bounce wave. As illustrated in Fig. 29, the diffraction of a line source field (i.e., the first-bounce field) by a ground plane guide consists of two components. The second-bounce field $H_T^{(2)}$ may be thought of as composed of the sum of the ground-plane reflected geometrical optics field $H_G^{(2)}$ and the diffracted field $H_S^{(2)}$ from a rectangular wall of width (a). $H_G^{(2)}$ is given by

(67) $H_G^{(2)} = \dfrac{e^{-jk\rho' + j\frac{\pi}{4}}}{\sqrt{2\pi\rho'}} \; I_{eq}^{(1)}$
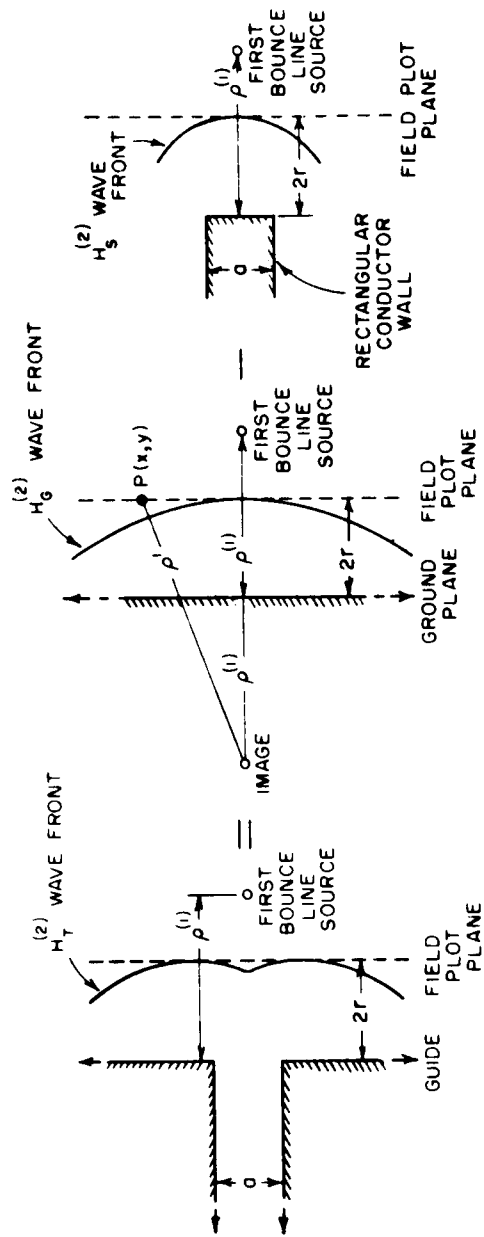
Fig. 24. Application of superposition to line source field diffraction by a ground-plane guide aperture.

60

where ρ' is the distance from the line source image to an observation point $P(x, y)$ on the field plot plane and $I_{eq}^{(1)}$ is the first-bounce wave equivalent line source current from Eq. (57). The other cylindrical wave component is given by

$$(68) \qquad H_S^{(2)} = H_G^{(2)} - H_T^{(2)} \ ,$$

where the total second-bounce wave $H_T^{(2)}$ is given by Eq. (66). It should be noted again that both Eqs. (67) and (68), like Eq. (66), describe field plots, not just discrete field values.

The second-bounce wave components $H_G^{(2)}$ and $H_S^{(2)}$ are both cylindrical. By superposition, they constitute the second-bounce cylindrical component waves incident on the guide aperture caused by the first-bounce wave. The contributions of $H_G^{(2)}$ and $H_S^{(2)}$ to the reflection coefficient are computed in the same way as is $\Gamma^{(1)}$ (Eq. (59)), the first-bounce cylindrical wave reflection coefficient component. For both $H_G^{(2)}$ and $H_S^{(2)}$, the same geometry for equivalent line source determination in Fig. 27 applies except for superscript changes.

For $H_G^{(2)}$ the line source location from the guide aperture, denoted by $\rho^{(2)}(1)$, is given by Eq. (56), with $\triangle \phi$ being the phase difference between $H_G^{(2)}$ (aperture center) and $H_G^{(2)}$ (edge). The equivalent line source current is given by

(69) $\qquad I_{eq}^{(2)}(1) = \sqrt{2\pi \rho^{(2)}(1)} \ e^{jk\rho^{(2)}(1) - j\frac{\pi}{4}}$

$$\times \ H_G^{(2)} \ \text{(aperture center)}.$$

Coupling back into the guide is given by

(70) $\qquad I_R^{(2)}(1) = I_{eq}^{(2)}(1) \ \sqrt{\dfrac{\lambda}{2\pi a}} \ H_T(\rho^{(2)}(1)) \ ,$

where $H_T(\rho^{(2)}(1))$ is the free-space guide magnetic field at $\rho^{(2)}(1)$

according to Eq. (17). Thus the reflection coefficient contribution

due to $H_G^{(2)}$ is given by

(71) $\qquad \Gamma^{(2)}(1) = \dfrac{I_{eq}^{(2)}(1)}{a} \ \sqrt{\dfrac{\lambda}{2\pi}} \ H_T(\rho^{(2)}(1)) \ .$

Similarly, for $H_S^{(2)}$ the reflection coefficient contribution is

given through the following equations:

(72) $\qquad \rho^{(2)}(2) = \dfrac{a^2}{8\Delta\phi} - \dfrac{\Delta\phi}{2} \ ,$

where $\Delta\phi$ is the phase difference between $H_S^{(2)}$ (aperture center) and

$H_S^{(2)}$ (edge);

(73) $\qquad I_{eq}^{(2)}(2) = \sqrt{2\pi \rho^{(2)}(2)} \ e^{jk\rho^{(2)}(2) - j\frac{\pi}{4}}$

$$\times \ H_S^{(2)} \ \text{(aperture center)};$$

62

$$(74) \qquad I_R^{(2)}(2) = I_{eq}^{(2)}(2) \sqrt{\frac{\lambda}{2\pi a}} \; H_T(\rho^{(2)}(2)) \; ;$$

and

$$(75) \qquad \Gamma^{(2)}(2) = \frac{I_{eq}^{(2)}(2)}{a} \sqrt{\frac{\lambda}{2\pi}} \; H_T(\rho^{(2)}(2)) \; .$$

It should be again noted that $H_T(\rho)$ in both Eqs. (71) and (75), as in Eq. (59), are computed by Eq. (17) for a free-space guide at a distance ρ from the aperture along the guide axis. The total contribution to the reflection coefficient from the second-bounce wave is then given by

$$(76) \qquad \Gamma^{(2)} = \Gamma^{(2)}(1) + \Gamma^{(2)}(2) \; .$$

3. Multiple-bounce waves

Similar to the generation of the two cylindrical wave components of the second-bounce wave by the first-bounce cylindrical wave, $H_G^{(2)}$ and $H_S^{(2)}$ each generates two cylindrical waves to constitute the third-bounce wave. The waves generated by $H_G^{(2)}$ is denoted by $H_G^{(3)}(1)$ and $H_S^{(3)}(1)$ while $H_G^{(3)}(2)$ and $H_S^{(3)}(2)$ represent the waves generated by $H_S^{(2)}$. Computational procedures for these generated components of $H_G^{(2)}$ and $H_S^{(2)}$ are exactly the same as those for computing $H_G^{(2)}$ and $H_S^{(2)}$ from the first-bounce cylindrical wave $H_T^{(1)}$. This cause-and-effect relationship for multiple-bounce wave generation can thus be extended to include any number of bounces. In general, the logic

diagrammed in Fig. 30 describes the generation of the cylindrical

components of the higher-order bounce waves. Thus by continuing

this process, any desired number of bounces may be included.

The total reflection coefficient is given in general by

$$(77) \qquad \Gamma_T = \Gamma_0 + \sum_{n=1}^{\infty} \Gamma^{(n)} \ (2n),$$

where Γ_0 is the self reflection coefficient computed by Eq. (30) and

(n) is the order of the bounce.

B. Results

The total reflection coefficient for the ground-plane guide

illuminating a perfectly conducting sheet was calculated by use of

a Scatran program on the IBM 7094. The logic of the program is

essentially the same as the block diagram shown in Fig. 30.

Computational rigor was reduced by the use of a DOTHROUGH loop

for the computation of the cylindrical wave generation and its coupling

into the guide. The results were computed for a ground-plane guide of

0.278λ guide width with the reflecting plate distance (r) varying from

0.5λ to 2.5λ. Five bounces were used for this computation.

Computing time on the IBM 7094 for the program is approxi-

mately one minute for each reflection sheet position. In order to

obtain a detailed plot of Γ_T as a function of reflecting plate distance

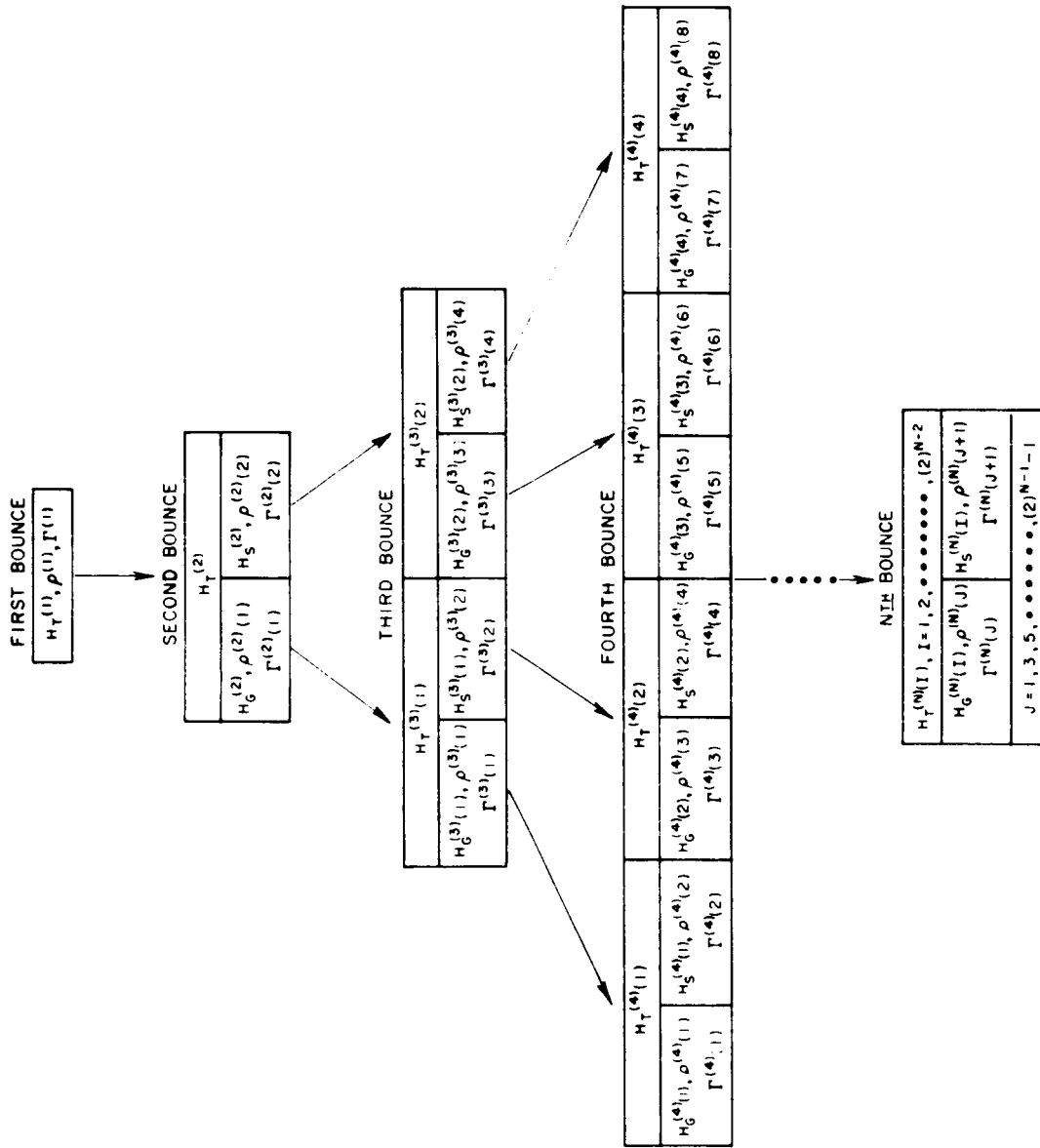(r), (r) would have had to be incremented every 0.05λ. This

64

Fig. 30. Multiple bounce generation "Tree" logic.

65

computational expense would have been too costly, consequently

a more economical scheme was used. From sample calculations at

selected reflecting plate distances, it was noticed that each bounce-

wave reflection coefficient contribution (namely $\Gamma^{(1)}$, $\Gamma^{(2)}$, $\Gamma^{(3)}$, and

..., etc.), when plotted versus the reflecting distance (r), exhibits

a magnitude variation very close to an exponential decay and a

phase variation very nearly linear. By calculating the reflection

coefficient at these widely spaced reflecting plate distances, the

exponential decays of the magnitudes of the various Γ components

and their corresponding linear phase variations were determined

by curve fitting approximations. These curves describe the com-

plex bounce-wave reflection coefficient components ($\Gamma^{(1)}$, $\Gamma^{(2)}$, ...,

etc.) as continuous functions of (r). The phasor sum of these Γ

component curves with Γ_O then yields the continuous total reflection

coefficient curve with a minimum expenditure of computer time.

The individual bounce-wave reflection coefficient magnitudes

calculated by the computer program for discrete reflecting plate

distances are shown in Fig. 31 with the exponential curves used to

approximate them. The apparent differences between the calculated

points and the approximation curves for the third and fourth bounces

result from inaccuracies in the computational procedure. For

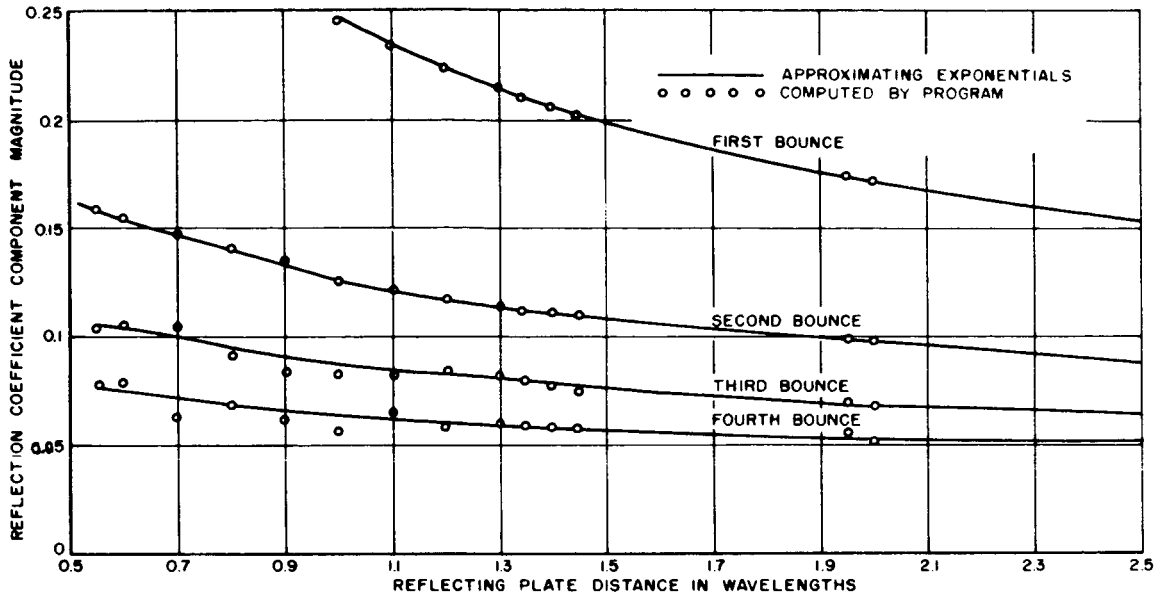example, for the fourth-bounce fields, eight components must be

Fig. 31. Bounce wave reflection coefficient magnitudes.

considered. Any error in the assumptions in the analysis or

computational inaccuracies are thus taken into account eight times

in the course of computation. The phase variation for the various

bounce components of Γ_T is $4n\pi$ radians per λ in (r), the reflecting

sheet distance, where (n) is the order of the bounce.

Experimental verification was obtained through the sectoral

horn of Fig. 14 with the horn aperture mounted in a ground plane.

Calculated-versus-measured results for a 0.278λ wide guide are

shown in Figs. 32-35. Figure 32 shows two sets of measured

results versus the calculated total reflection coefficient magnitude

which includes the first four bounces. Figure 33 shows the calculated

results for Γ_T by separately including one, two and then three

67

bounces. Bounce contributions to the total reflection coefficient are seen to behave as harmonic components. Figure 34 compares Γ_T with four and five bounces included in the computation. From Fig. 34, the effect on Γ_T by including the fifth-bounce is seen to be quite small. The computed phase of the total reflection coefficient, including the first four bounces, is presented in Fig. 35.
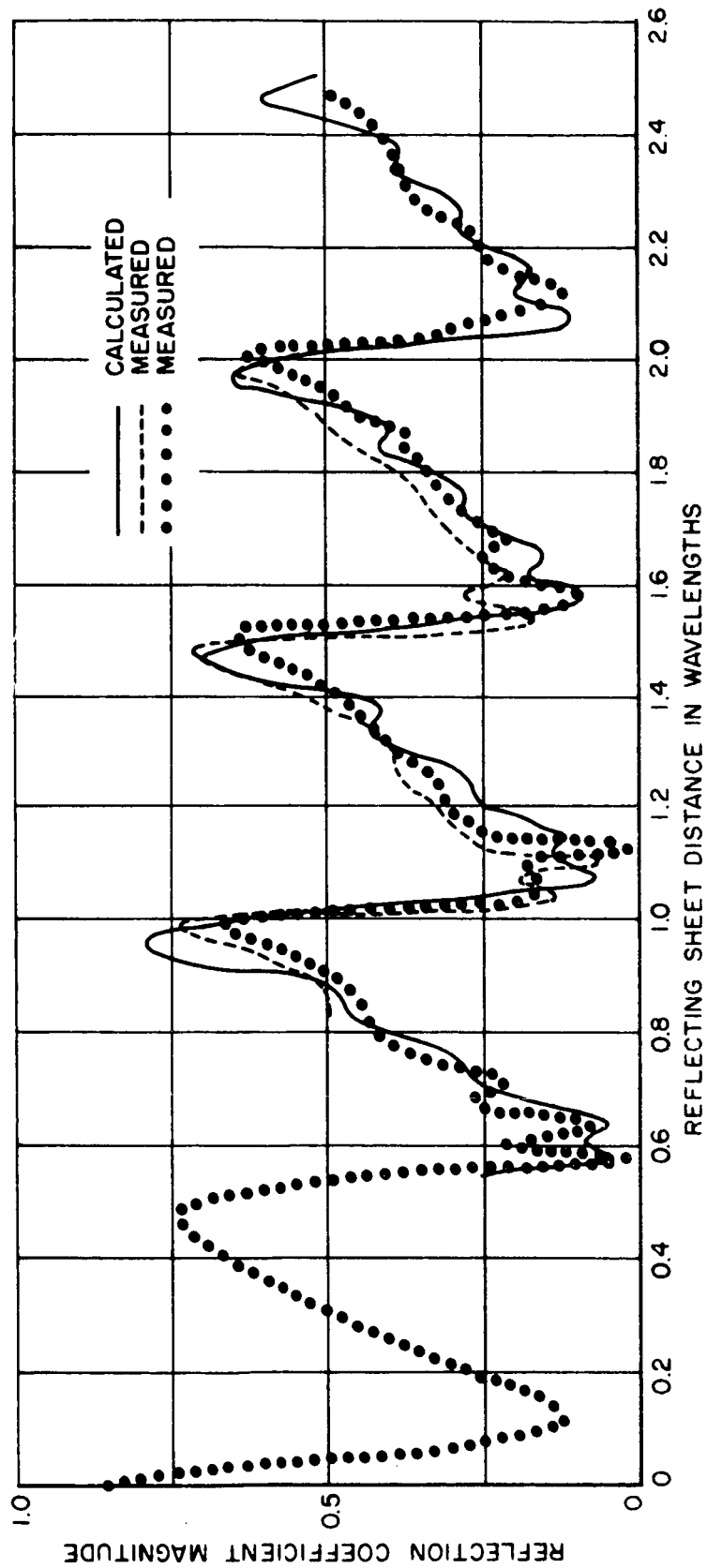
Fig. 32. The reflection coefficient magnitude for a ground plane guide illuminating a reflecting sheet including the first four bounces.
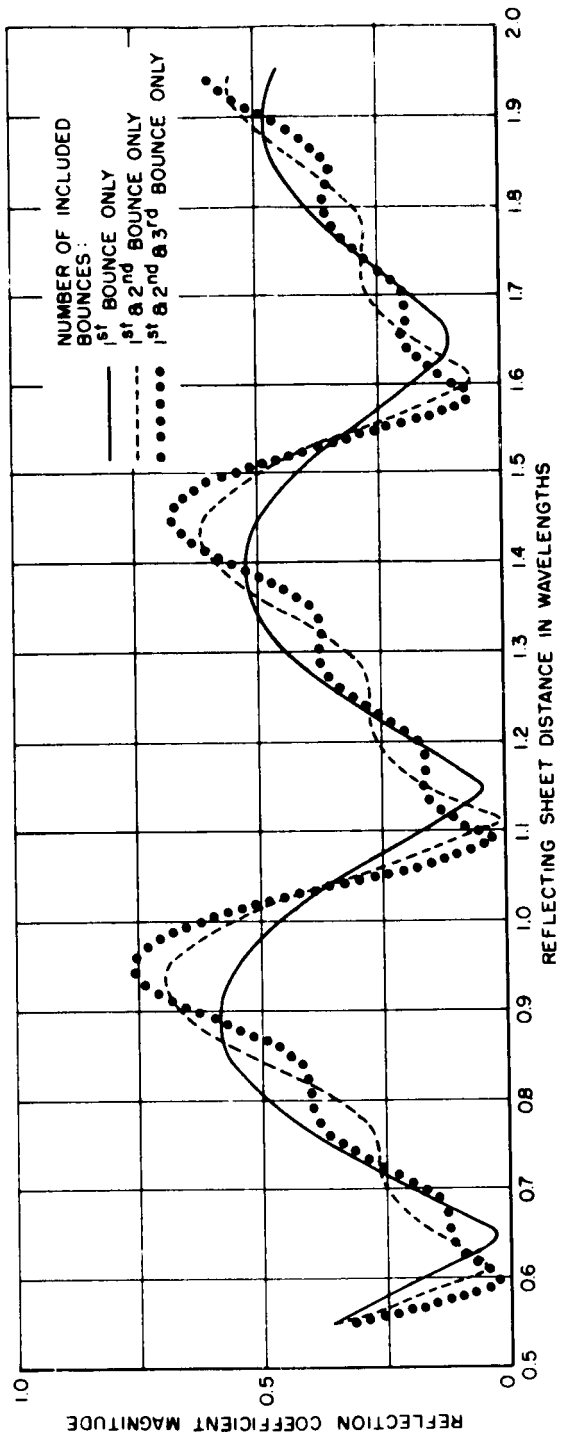
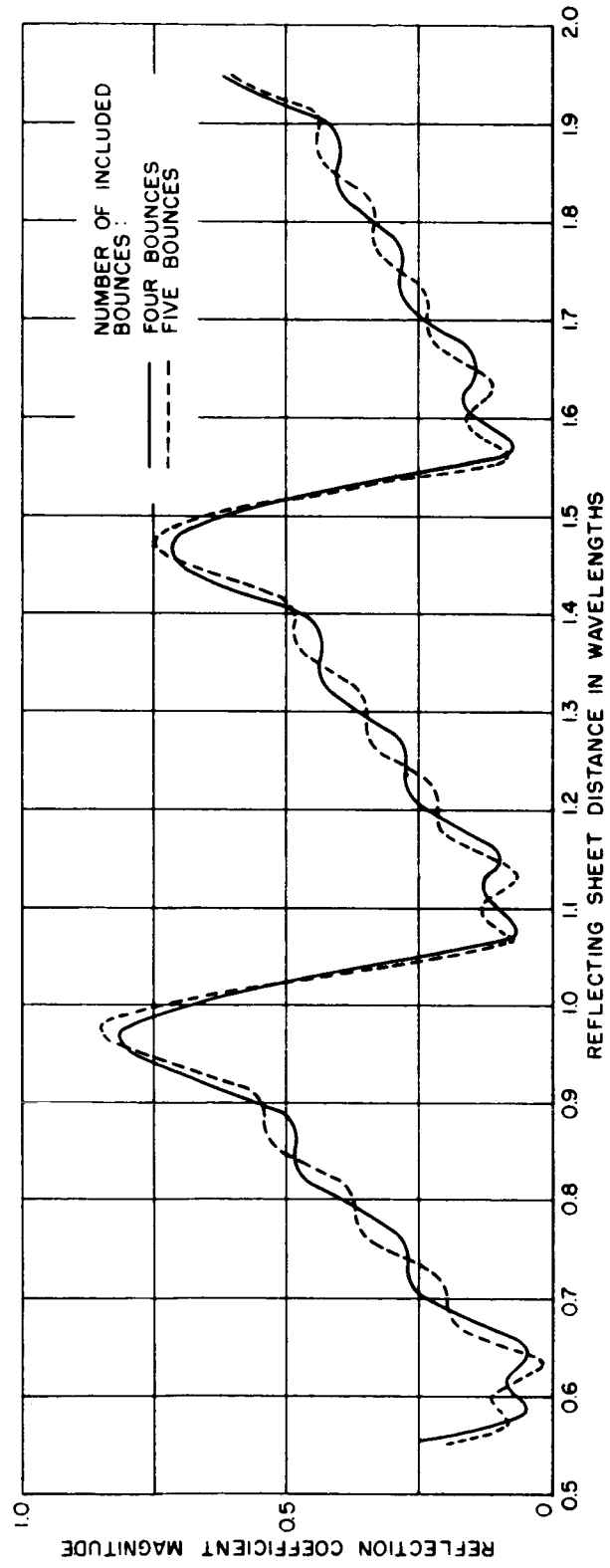Fig. 33. Γ_T magnitude with one, two, and three bounces.

70

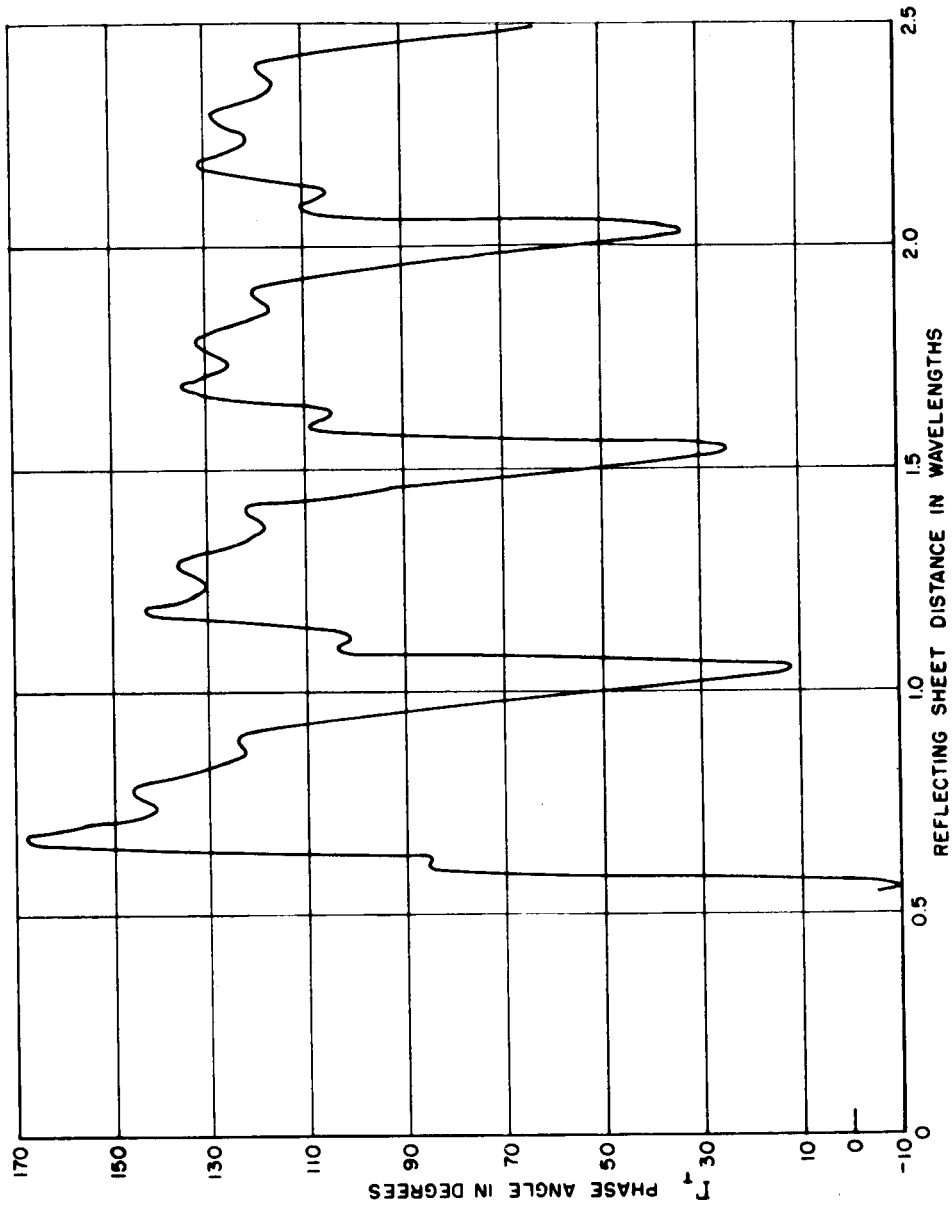Fig. 34. Γ_T magnitude with four and five bounces.

71

Fig. 35. Γ_T phase by including the first four bounces.

72

CHAPTER VI
SUMMARY AND CONCLUSIONS

The reflection coefficient of a parallel-plate waveguide operating in the TEM mode and illuminating a perfectly reflecting sheet has been analyzed as a function of guide aperture to reflector distance through wedge diffraction techniques. For the half-plane guide (zero wedge angle), the reflection coefficient was obtained through integration over the guide cross section of the magnetic field reflected back from the reflecting sheet onto the guide aperture. Experimental verification was obtained for this case using a narrow-angle sectoral horn. Good agreement was found between calculated and measured results.

For guides with finite wedge angles less than $90°$, the interactions between the guide aperture and the reflecting sheet were approximated by bouncing plane waves. The total fields resulting from these plane waves were obtained through applications of the Higher-Order Diffraction Concept.[7] General agreement between measured and calculated reflection coefficient magnitudes was obtained. However, the verification is not conclusive because the self reflection coefficient of the chosen guide geometry was found to be quite high. It should be noted that though symmetry in wedge angles

was assumed in the analysis, asymmetry may be tolerated provided the primary assumption that the interactions between the guide and the reflector are plane waves is not violated by this asymmetry in wedge angles.

For ground-plane mounted guides (90° wedge angles), the assumption that the interactions between the guide and the reflector may be approximated by bouncing plane waves was found to be invalid because of the presence of reflection boundaries in the directions of interest. Consequently, the exact nature of each bounce wave was taken into account in a method of successively bouncing cylindrical waves. An iterative computational procedure was used to find the various reflection coefficient contributions from each individual bounce. Again, good agreement between measured and calculated results was obtained.

For each of the above cases, the normalized admittances may be obtained from their corresponding reflection coefficients by

$$(78) \qquad \frac{Y_T}{Y_o} = \frac{1 - \Gamma_T}{1 + \Gamma_T} \qquad ,$$

where Y_o is the admittance of free space.

Since the ultimate purpose of this analysis is to gain insight for antenna applications in reflectometer systems, a non-oscillatory reflection coefficient magnitude versus reflector distance curve is

74

desired. This analysis has shown that the oscillatory behavior of most curves thus far obtained is due to the phasor addition properties of the summation of the antenna's self reflection coefficient and the various bounce waves' reflection coefficient contributions. The self reflection coefficient presents little difficulty in practical applications because it may be easily minimized through design considerations. However, for the practical ground-plane mounted antenna, the significance of multiple bounce waves between the ground-plane and the reflecting sheet cannot be over-looked. The presence of these bounce waves will always cause the reflection coefficient magnitude versus reflecting sheet distance curve to be oscillatory. Therefore, in order to use a ground-plane mounted antenna in a reflectometer system, higher-order interactions between the ground-plane and the reflecting sheet must be taken into account.

APPENDIX A

The diffraction function $V_B(r, \phi, n)$ for plane wave incidence has been expressed by Pauli[2] as

$$
(79) \qquad V_B(r, \phi, n) = \frac{1}{\sqrt{\pi}} \; \frac{\sin\frac{\pi}{n} \; e^{j\frac{\pi}{4}}}{n} \; \frac{2 \left|\cos\frac{\phi}{2}\right|}{\cos\frac{\pi}{n} - \cos\frac{\phi}{n}}
$$

$$
\times \; e^{jkr\cos\phi} \int_{[(1+\cos\phi)kr]^{\frac{1}{2}}}^{\infty} e^{-j\tau^2} \, d\tau
$$

$$
+ \; [\text{higher order terms}] \; .
$$

The higher-order terms in Eq. (79) are identically equal to zero for the half-plane case, i.e., $n = 2$. For more general values of n, the higher-order terms are negligible for large values of kr. The function may be further simplified for large values of $(1 + \cos\phi)\,kr$; large values of $(1 + \cos\phi)kr$ imply that the point of observation is removed from both the diffracting wedge (r large) and the shadow boundary ($\phi = 180° \; \longrightarrow \; 1 + \cos\phi = 0$). The field, under these conditions, may be expressed by

76

$$(80) \qquad V_B(r, \phi, n) = \frac{e^{-j\left(kr + \frac{\pi}{4}\right)}}{\sqrt{2\pi kr}} \quad \frac{\frac{1}{n} \sin \frac{\pi}{n}}{\cos \frac{\pi}{n} - \cos \frac{\phi}{n}}$$

$$+ [\text{ higher-order terms}] .$$

The diffracted field as expressed by Eq. (80) is that from which the asymptotic diffraction coefficients of the Geometrical Theory of Diffraction[2] are obtained.

For cases in which the higher-order terms of Eq. (79) are significant, an alternative formulation of the problem based on a Bessel function expansion given in Reference 12 may be used. For example, the higher-order terms of the Fresnel integral formulation become significant for values of the radial parameter r less than one wavelength in the case of the 90° wedge. The Bessel function formulation, which converges rapidly for radial parameters in this region, is given by

$$(81) \qquad V(r, \phi, n) = \frac{1}{n} \sum_{m=0,1}^{\infty} \epsilon_m \, j^{\frac{m}{n}} \, J_{\frac{m}{n}}(kr) \times \cos \frac{m\phi}{n} ,$$

where $J_{\frac{m}{n}}(kr)$ is the cylindrical Bessel function of order m/n and ϵ_m is Neumann's number defined by

$$\epsilon_m = \begin{cases} 1 & m = 0 \\ 2 & m \neq 0 \end{cases} .$$

Equation (81) represents the total incident or reflected field where the total field is given by

$$(82) \qquad U(r, \psi, n) = V(r, \psi - \psi_o, n) \pm V(r, \psi + \psi_o, n) .$$

The diffracted field may be obtained by simply subtracting the geometric optics field in Eq. (3) from the expression in Eq. (81).

REFERENCES

1. Sommerfeld, A., Optics, Academic Press, (1964),
    pp. 249-266.

2. Pauli, W., "An Asymptotic Series for Functions in the Theory
    of Diffraction of Light," Phys. Rev., 54 (1 December 1938),
    pp. 924-931.

3. Obha, Y., "On the Radiation Patterns of a Corner Reflector
    Finite in Width," IRE Trans. on Antennas and Propagation,
    AP-11, No. 2 (March 1963), pp. 127-132.

4. Russo, P.M., Rudduck, R.C., and Peters, L. Jr., "A
    Method for Computing E-Plane Patterns of Horn Antennas,"
    IEEE Trans. on Antennas and Propagation, AP-13, No. 2
    (March 1965), pp. 219-224.

5. Tsai, L.L., and Rudduck, R.C., "Accuracy of Approximate
    Formulations for Near-Field Wedge Diffraction of a Line
    Source," Report 1691-18, 15 March 1966, Antenna Laboratory,
    The Ohio State University Research Foundation; prepared
    under Grant NsG-448, National Aeronautics and Space
    Administration, Office of Grants and Research Contracts,
    Washington, D.C.

6. Rudduck, R.C., "Application of Wedge Diffraction to Antenna
    Theory," Report 1691-13, 30 June 1965, Antenna Laboratory,
    The Ohio State University Research Foundation; prepared
    under Grant NsG-448, National Aeronautics and Space
    Administration, Office of Grants and Research Contracts,
    Washington, D.C.

7. Rudduck, R.C., and Yu, J.S., "Higher-Order Diffraction
    Concept Applied to Parallel-Plate Waveguide Patterns,"
    Report 1691-16, 15 October 1965, Antenna Laboratory,
    The Ohio State University Research Foundation, prepared
    under Grant NsG-448, National Aeronautics and Space
    Administration, Office of Grants and Research Contracts,
    Washington, D.C.

8. Dybdal, R.B., Rudduck, R.C. and Tsai, L.L., "Mutual
    Coupling Between TEM and TE_{01} Parallel-Plate Waveguide
    Apertures," to be published in IEEE Transactions on Antennas
    and Propagation.

9. Yu, J.S., R.C. Rudduck, and L. Peters, Jr., "Comprehensive
    Analysis for E-Plane of Horn Antennas by Edge Diffraction
    Theory," IEEE Transaction on Antennas and Propagation,
    AP-14, (March 1966), pp. 138-149.

10. Tsai, L.L., Rudduck, R.C., "Aperture Reflection Coefficient of Parallel-Plate Waveguides by Wedge Diffraction Analysis," (Antenna Laboratory Report in Preparation).

11. Ryan, C.E., Jr., and Rudduck, R.C., "Calculation of the Radiation Pattern of a General Parallel-Plate Waveguide Aperture for the TEM and TE_{01} Waveguide Modes," Report 1693-4, 10 September 1964, Antenna Laboratory, The Ohio State University Research Foundation; prepared under Contract N62269-2184, U.S. Naval Air Development Center, Johnsville, Pennsylvania.

12. Harrington, R.F., Time-Harmonic Electromagnetic Fields, McGraw-Hill Book Company, Inc., New York (1961) pp. 238-242.